EBioMedicine 74 (2021) 103725

Contents lists available at ScienceDirect

EBioMedicine

journal homepage: www.elsevier.com/locate/ebiom

Phospholipid nanoparticles: Therapeutic potentials against atherosclerosis via reducing cholesterol crystals and inhibiting inflammation

Yonghong Luo[a,b,†], Yanhong Guo[a,†,*], Huilun Wang[a], Minzhi Yu[c], Kristen Hong[c], Dan Li[c], Ruiting Li[c], Bo Wen[c], Die Hu[b], Lin Chang[a], Jifeng Zhang[a], Bo Yang[e], Duxin Sun[c], Anna S. Schwendeman[c,d,**], Y. Eugene Chen[a,e,***]

[a] Department of Internal Medicine, Cardiovascular Center, University of Michigan Medical School, Ann Arbor, MI 48109, USA
[b] Second Xiangya Hospital, Central South University, Hunan Province, China
[c] Department of Pharmaceutical Sciences, College of Pharmacy, University of Michigan, Ann Arbor, MI 48109, USA
[d] Biointerfaces Institute, University of Michigan, Ann Arbor, MI, USA
[e] Department of Cardiac Surgery, University of Michigan Medical School, Ann Arbor, MI, USA

ARTICLE INFO

Article History:
Received 13 July 2021
Revised 14 November 2021
Accepted 16 November 2021
Available online xxx

Keywords:
Atherosclerosis
Nanoparticle
Cholesterol crystal
HDL
Inflammation

ABSTRACT

Background: Atherosclerosis-related cardiovascular diseases (CVDs) are the leading cause of mortality worldwide. Cholesterol crystals (CCs) induce inflammation in atherosclerosis and are associated with unstable plaques and poor prognosis, but no drug can remove CCs in the clinic currently.
Methods: We generated a phospholipid-based and high-density lipoprotein (HDL)-like nanoparticle, miNano, and determined CC-dissolving capacity, cholesterol efflux property, and anti-inflammation effects of miNano *in vitro*. Both normal C57BL/6J and *Apoe*-deficient mice were used to explore the accumulation of miNano in atherosclerotic plaques. The efficacy and safety of miNano administration to treat atherosclerosis were evaluated in the *Ldlr*-deficient atherosclerosis model. The CC-dissolving capacity of miNano was also detected using human atherosclerotic plaques *ex vivo*.
Findings: We found that miNano bound to and dissolved CCs efficiently *in vitro*, and miNano accumulated in atherosclerotic plaques, co-localized with CCs and macrophages *in vivo*. Administration of miNano inhibited atherosclerosis and improved plaque stability by reducing CCs and macrophages in *Ldlr*-deficient mice with favorable safety profiles. In macrophages, miNano prevented foam cell formation by enhancing cholesterol efflux and suppressed inflammatory responses *via* inhibiting TLR4-NF-κB pathway. Finally, in an *ex vivo* experiment, miNano effectively dissolved CCs in human aortic atherosclerotic plaques.
Interpretation: Together, our work finds that phospholipid-based and HDL-like nanoparticle, miNano, has the potential to treat atherosclerosis by targeting CCs and stabilizing plaques.
Funding: This work was supported by the National Institutes of Health HL134569, HL109916, HL136231, and HL137214 to Y.E.C, HL138139 to J.Z., R21NS111191 to A.S., by the American Heart Association 15SDG24470155, Grant Awards (U068144 from Bio-interfaces and G024404 from M-BRISC) at the University of Michigan to Y.G., by the American Heart Association 19PRE34400017 and Rackham Helen Wu award to M. Y., NIH T32 GM07767 to K. H., Barbour Fellowship to D.L.

1. Introduction

CVDs are the leading cause of mortality worldwide, most of which are contributed by a heart attack and stroke due to atherosclerosis [1,2]. Atherosclerosis is a chronic inflammatory disease initially induced by low-density lipoprotein cholesterol (LDL-C) retention in the arterial wall [3]. Although lipid-lowering drugs substantially prevent cardiovascular events in atherosclerosis [2,4], some patients still

* Corresponding author at: Yanhong Guo, M.D., Ph.D., Department of Internal Medicine, University of Michigan Medical School, Ann Arbor, MI 48109, USA.
** Corresponding author at: Anna S Schwendeman, Ph.D., Department of Pharmaceutical Sciences, College of Pharmacy, University of Michigan, Ann Arbor, MI 48109, USA.
*** Corresponding author at: Y. Eugene Chen, M.D., Ph.D., Department of Internal Medicine, University of Michigan Medical School, Ann Arbor, MI 48109, USA.
E-mail addresses: yanhongg@umich.edu (Y. Guo), annaschw@umich.edu (A.S. Schwendeman), echenum@umich.edu (Y. Eugene Chen).
† These authors share the first author position: Yonghong Luo and Yanhong Guo.

https://doi.org/10.1016/j.ebiom.2021.103725

Research in context

Evidence before this study

Atherosclerosis contributes to most cardiovascular diseases (CVDs), which are the leading cause of mortality worldwide. Cholesterol crystals (CCs) induce inflammation in atherosclerosis and are associated with unstable plaques and poor prognosis. Drugs that can remove CCs or prevent CC formation may provide new strategies to treat atherosclerosis. However, no drug can remove CCs in the clinic currently.

Added value of this study

We developed a phospholipid nanoparticle, miNano, which shows biological function as a CC dissolving agent and cholesterol acceptor in the cholesterol efflux process. miNano had the most robust CC-dissolving ability compared to HDL and cyclodextrin. miNano accumulated in atherosclerotic plaques. Using the *Ldlr*-deficient mouse model, we demonstrated that administration of miNano inhibited atherosclerosis and improved plaque stability by reducing CCs and macrophages with favorable safety profiles. We also demonstrated that miNano prevented foam cell formation by enhancing cholesterol efflux and suppressed inflammatory responses *via* inhibiting TLR4-NF-κB pathway in macrophages.

Implications of all the available evidence

Our data strengthen the importance of developing and exploring innovative and new treatment strategies for atherosclerosis by modulating components in plaques and counteracting CC-induced inflammation. Our findings provide a novel approach for developing phospholipid-based miNano as a promising option to alleviate plaque burden and treat atherosclerosis.

suffer from high residual risk despite a dramatic reduction in LDL-C [5,6]. Anti-inflammation therapy has been pursued to decrease cardiovascular events further. However, only two strategies among various anti-inflammation treatments, canakinumab, a human monoclonal antibody against interleukin-1 beta (IL-1β), and colchicine, have shown beneficial effects in large clinical trials [7–11]. One of the potential explanations is that other therapeutic agents failed to reduce residual inflammatory stimuli such as CCs in the plaques.

Originated from the excess LDL-C that has penetrated the arterial wall [12,13], CCs appear early and accumulate along time within plaques [14–16], making it a characteristic of atherosclerosis. CCs induce inflammation in various cells *via* multiple pathways in atherosclerotic plaques. Atherosclerotic CCs stimulate neutrophils to form neutrophil extracellular traps (NETs), exaggerating immune response [17]. CCs can also directly activate the NLRP3 inflammasome in macrophages, resulting in the release of pro-inflammatory IL-1β [15,18]. Furthermore, crystallization of liquid cholesterol causes volume expansion, leading to mechanical vascular injury by plaque erosion or rupture [19]. Abundant evidence has shown that CCs are related to vulnerable plaques and poor prognosis [20–26]. Hence, new drugs that can remove CCs or prevent CC formation may provide new strategies to prevent atherosclerosis development, stabilize plaque, and reduce cardiovascular events.

Lipid-lowering drugs are estimated to reduce CCs in plaques due to the overall lower circulation cholesterol level [27], but direct evidence lacks in clinical studies. 2-hydroxypropyl-β-cyclodextrin (HPBCD), a cyclic oligosaccharide, is a promising treatment for Niemann-Pick type C disease by reducing lysosome lipid accumulation [28]. HPBCD has been reported to dissolve CCs and promote atherosclerosis regression in mice [29]. However, hearing loss is reported to be associated with HPBCD treatment [30,31] due to the role of propyleneglycol in HPBCD or outer hair cell death induced by high dose of HPBCD [32–34]. High-density lipoprotein (HDL) exerts multiple protective roles against atherosclerosis [35]. However, raising HDL levels and administration of reconstituted HDLs (rHDLs) have not shown further beneficial effects on top of cholesterol-lowering treatments [5,36–38]. Recently, our and others' studies have demonstrated that components of synthetic HDLs (sHDLs) particles greatly affect their functions [39] and that different phospholipids and proteins in sHDLs exert differential impacts on the capacity of cholesterol efflux and anti-inflammation [40–42]. Importantly, HDL particles can dissolve CCs and inhibits CC-induced inflammatory responses [43,44], albeit few studies have focused on this property.

Based on the structure of HDL and previous studies [41,45–47], we developed a phospholipid-based nanoparticle (NP), namely Michigan Nanoparticle (miNano), which is directly bound to CCs and dissolved CCs more robustly than HDL and HPBCD do. *In vivo,* we demonstrated that miNano accumulated in atherosclerotic plaques, inhibited atherosclerosis, and stabilized plaques in *Ldlr*-deficient mice by reducing CCs and macrophage infiltration. Mechanism study indicated that miNano prevented foam cell formation *via* enhancing cholesterol efflux and suppressing inflammatory responses via inhibiting TLR4-NF-κB pathway in macrophages. Moreover, miNano is capable of dissolving CCs in human atherosclerotic plaques *ex vivo*. Our study provides a new treatment strategy for atherosclerosis by modulating components in plaques, counteracting CC-induced inflammation, and stabilizing plaques.

2. Methods

2.1. Animals

C57BL/6J (RRID:IMSR_JAX:000664), *Apoe*-deficient (B6.129P2-*Apoe*^{tm1Unc}/J, RRID:IMSR_JAX:002052), or *Ldlr*-deficient mice (B6.129S7-*Ldlr*^{tm1Her}/J, RRID:IMSR_JAX:002207) of 7, 8 weeks old were bought from Jackson Laboratories. All animal procedures were performed according to protocols approved by the Institutional Animal Care & Use Committee (IACUC) at the University of Michigan. C57BL/6J mice were fed ad libitum with a standard laboratory diet (LabDiet, 13% of calories from fat). For atherosclerosis studies [46,48], *Apoe*-deficient or *Ldlr*-deficient mice were fed on a western diet (ENVIGO, 42% of calories from fat and 0.2% cholesterol) ad libitum for 12 weeks. In the biodistribution study [46], one dose of vehicle or 250 mg/kg DiD-miNano was given either to C57BL/6J or *Apoe*-deficient atherosclerotic mice, and then mice were sacrificed 24 h after injection. In the atherosclerosis treatment study, after 12-week western diet, animals were switched to a standard laboratory diet and were randomly divided into four groups to be either sacrificed as baseline or to be treated with vehicle, 250 mg/kg miNano, or 400 mg/kg HPBCD via tail vein injection twice a week for 6 weeks [41,46]. To minimize potential confounders such as body weight, randomization was achieved by random-numbers table based on body weight. Samples were harvested 48 h after the last dosage of treatment. Aorta was collected for plaque quantification. Aortic sinus was sectioned for plaque characterization. Blood, liver, kidney, heart, spleen, lung, and small intestine were harvested for safety analysis. Animals were housed up to 5 mice/cage with a 12 h-light/12 h-dark circadian. For each study, samples were analyzed altogether to avoid batch bias. Sample sizes (n = 10 for each group) were determined using G*Power 3 software [49] and based on previous studies in our laboratory, enabling power of 0.9 and $p < 0.05$. Animal was excluded from analysis if died before endpoint. No outlier is excluded for in vivo studies. Investigators were not blinded during conducting the experiment but were blinded during the allocation, sample collection, and data analysis.

2.2. Preparation of sHDL and HDL-like NPs

Chemicals: 22A (PVLDLFRELLNELLEALKQKLK) was synthesized by Genscript (Piscataway, NJ). All the phospholipids and PEGylated lipids used to make sHDL and HDL-like NPs were purchased from NOF America Corporation.

Preparation of sHDL [41,50]: Briefly, ApoA-1 mimetic peptide 22A and phospholipids (DMPC, DLPC, POPC, or DPPC) were dissolved and mixed in acetic acid, followed by lyophilized for 24 h (mass ratio of 22A: lipids = 1:2). The lyophilized powders will be rehydrated by PBS (pH = 7.4). Three heat-cooling cycles above and below lipid transition temperatures will be performed to form sHDL particles. Dynamic Light Scattering (DLS) was used to examine the particle size.

Preparation of HDL-like NPs: Briefly, HDL-like NPs were prepared by dissolving DPPC and DSPE-PEG2k/DSPE-PEG5k in glacial acetic acid at different molar ratios indicated by Table S1. After freeze-drying for over 24 h, PBS (pH = 7.4) was added to hydrate the powders. The mixture was sonicated briefly, heated to 50 °C for 10 min, and cooled to room temperature for 10 min. This cycle was repeated three times. The miNano solution was stored at -20 °C till use. miNano was prepared as described above, with the composition being DPPC and DSPE-PEG2k and the molar ratio at 1:2. The particle size was determined by DLS, and the morphology was observed by transmission electron microscopy (TEM) as described previously [41,50]. Briefly, miNano solution was diluted and deposited on a carbon film-coated 400 mesh copper grid (Electron Microscopy Sciences) and dried for 1 min. Samples were then negatively stained with 1% (w/v) uranyl formate, and the grid was dried before TEM observation. All specimens were imaged on a 100kV Morgagni TEM equipped with a Gatan Orius CCD.

DiD-miNano and Rhodamine PE-miNano preparation [45,46]. DiD-miNano and Rhodamine PE-miNano were prepared in the same way as miNano except that before rehydrating, DiD dye (Thermo Fisher, D307) or 16:0 Liss Rhodamine PE (Avanti, 810158) was added to the DPPC and DSPE-PEG2k mix to a final concentration of 0.03% (w/w) for DiD-miNano and 10% (w/w) for Rhodamine PE-miNano. The particle size was determined by DLS.

2.3. Preparation of CCs

2 mg/ml cholesterol (Sigma, C8667) solution or NBD-cholesterol (Invitrogen, N1148) solution was made in 100% ethanol. CCs or NBD-CCs were formed by mixing the cholesterol solution with a 1.5-time volume of sterile water followed by drying under 56 °C overnight. NBD-CCs were protected from light in the whole process.

2.4. CC-dissolving test

200 μg/well CCs were prepared in 96-well plates (Falcon, 353072). After drying, 200 μl indicated solutions were added to each well, and 4 μl supernatant was used for cholesterol detecting by Cholesterol E kit (Fujifilm, 999-02601) 24 and 72 h after incubation.

CCs were coated in 8-chamber culture slides (Falcon, 354108) to observe the CC shapes and structure after incubation with indicated solutions. The slides were imaged under a microscope at indicated time points.

2.5. The binding of NBD-CCs with miNano

To detect if miNano can directly bind with CCs, NBD-CCs were generated in 8-chamber culture slides and incubated with Rhodamine PE-miNano solution for one hour. After washing to remove unbound Rhodamine PE-miNano, the slides were imaged under a confocal microscope.

2.6. Cholesterol efflux assay [41,46]

J774A.1 cells were radiolabeled by incubating with 1 μCi/ml [^{3}H] cholesterol (PerkinElmer, NET139001MC) in DMEM (Gibco, 11995065) containing 0.3% fatty acid-free bovine serum albumin (BSA) (Sigma, A8806) and 5 μg/ml ACAT inhibitor Sandoz 58-035 (Sigma, S9318) overnight. After washing twice with PBS twice, J774A.1 cells were equilibrated with DMEM containing 0.3% BSA and 5 μg/ml Sandoz 58-035 overnight. Next, cells were incubated with indicated solutions in 0.3% BSA DMEM for 4 h at 37 °C. Cell culture medium was collected and centrifuged at 10000 rpm for one minute to remove detached cells. Cells were lysed with 1N sodium hydroxide solution (Fisher Scientific, SS266-4) for 2 h on an orbital shaker at 300 rpm at room temperature. [^{3}H] cholesterol of medium and cell lysis solution was detected using a liquid scintillation counting cocktail (RPI, 111175). Cholesterol efflux was calculated as medium counts / (medium counts + cell lysis counts) $\times$ 100%. PBS and commercial HDL (Alfa Aesar, J64903) were used as the negative and positive control, respectively.

2.7. Biodistribution of miNano [46]

One dose of vehicle or 250 mg/kg DiD-miNano was injected via tail vein to either C57BL/6J mice fed on a standard laboratory diet or *Apoe*-deficient mice fed on a western diet for 12 weeks. Twenty-four hours later, mice were sacrificed and perfused with 10 ml saline. Blood, heart, aorta, liver, kidney, spleen, lung, duodenum, adipose tissue, muscle, femur, and brain were collected in cold PBS protected from light. Blood and tissues were images by *in vivo* imaging system (IVIS) immediately, and the average radiant efficiency was quantitated. Aortas were then fixed in formalin (Fisherbrand, 245-685) overnight, protected from light, and stained with ORO staining. Images of stained aortas were collected using SPOT 5.2 software. Aortic sinus slides were sectioned and counterstained with DAPI and galectin 3. Images were taken under polarized light of fluorescent microscope and confocal microscope.

2.8. Histology and immunofluorescent stainings

2.8.1. Aortic sinus sections [46,51]

Frozen sections of the aortic sinus were processed for CC imaging, galectin-3 staining, and Masson's trichrome staining. Briefly, mice were sacrificed by CO_2 and then perfused with 10 ml normal saline followed by 10 ml formalin via the left ventricle. Hearts were collected and fixed in formalin for at least two weeks. Frozen heart tissues were sectioned at 7 μm thick from the appearance of any one of the aortic valves to the disappearance of all three valves. Sections were stored at -80 °C until staining.

2.8.2. Tissue sections

Frozen sections of the heart, liver, spleen, kidney, lung, and duodenum were used for H&E staining. Mice were sacrificed by CO_2 and perfused sequentially with normal saline and formalin. Heart, liver, spleen, kidney, lung, and duodenum were harvested and kept in formalin before sectioning. H&E staining of frozen sections of the heart, liver, lung, spleen, kidney, and duodenum was performed at the IVAC Histology Laboratory at the University of Michigan.

2.8.3. Galectin 3 staining

Aortic sinus sections were fixed with 4% (v/v) paraformaldehyde (Thermo Scientific, J19943-K2) in PBS for 15 min, followed by washing with PBS three times, then slides were incubated with blocking buffer (2% donkey serum [Sigma, D9663] with 0.3% Triton X-100 [Sigma, T8787]) for one hour at room temperature. Sections were then incubated with anti-galectin 3 antibody (Invitrogen, 50-5301-82) at 1:200 diluted in dilution buffer (1% donkey serum with 0.1%

Triton X-100) at 4 °C overnight. Sections were then washed in PBS three times and incubated with secondary antibody (Jackson ImmunoResearch, 712-585-153) at 1: 500 in dilution buffer for one hour at room temperature. After washing with PBS, sections were mounted with ProLong™ Gold antifade reagent with DAPI (Invitrogen, P36935), and images were taken under the fluorescent microscope under the same settings.

2.8.4. Masson's trichrome staining

Masson's trichrome staining of frozen aortic sinus sections was performed by the *In Vivo* Animal Core (IVAC) Histology Laboratory at the University of Michigan.

2.8.5. Oil Red O (ORO) staining of the aorta trees [46,48,51]

Aorta trees were carefully isolated and fixed in formalin at least overnight. Aorta trees were then stained in ORO solution (1.6 mg/ml ORO [Sigma, O0625] and 77.8% [v/v] methanol [sigma, 179337] in 1 N sodium hydroxide solution) for 50 min, incubated in 70% ethanol for 30 min and then kept in distilled water until imaging. Images were taken using SPOT 5.2 software under the same settings.

2.8.6. Quantification of atherosclerotic lesions [46,48,51]

Three aortic sinus sections with at least two intact valves were used for quantification to obtain an average value for each animal. CCs were determined under a polarized light microscope, and the macrophage area was defined as Galectin 3/Mac 2-positive area. Necrotic core (NC) was selected as a vacant area, and collagen area was determined as a blue-stained region in Masson's trichrome staining. For the aortic tree, the plaque area was determined by the red-stained area after ORO staining. Quantification of each section was achieved using Image J under the same settings.

2.9. Plasma analysis

Whole blood was withdrawn from mouse orbit upon the sacrifice and centrifuged at 6000 rpm for 15 min, after which plasma was collected and stored at -80 °C until analysis. Plasma ALT, AST, ALB, TBil, ALP, CREA, and BUN were detected by the IVAC Diagnostic Laboratory at the University of Michigan.

2.10. Fecal bile acids measurement

400 μL 80% methanol/water solution was added per 100 μg feces sample. The mixed solution was homogenized and centrifuged at 13500 rpm for 10 min. 30 μL of supernatant was dispensed into a 96-well plate; then 120 μL methanol and 10 μL internal standard solution were added and vortexed for 10 min. The plate was centrifuged at 3500 rpm for 10 min at 4 °C to precipitate protein. The supernatant of 100 μL were transferred to another injection 96-well plate and 5 μL was injected into LC-MS/MS for analysis.

2.11. Quantitative real-time PCR (qPCR) analysis

Total RNA from cells was extracted using RNeasy Mini Kit (Qiagen, 74106). Reverse transcription was performed using SuperScript III First-Strand (Invitrogen, 18080-051) with random primers. SYBR green fast qPCR mix (ABclonal, RM21203) was used to perform qPCR with specific gene primers (Table S2). $\Delta\Delta$Ct method was used to quantitate gene expression, which was normalized to *Ppia* (mouse) or *PPIA* (human).

2.12. Cells

2.12.1. Primary human coronary artery endothelial cells

Primary human coronary artery endothelial cells were obtained from Lonza (Catalog #: CC-2585). Cells were kept in EGM™ -2 MV Microvascular Endothelial Cell Growth Medium (Lonza, Catalog #: CC-3202) and passaged every three days.

2.12.2. Primary human aorta smooth muscle cells

Primary human aorta smooth muscle cells were obtained from Lonza (Catalog #: CC- 2571). Cells were kept in SmGM™- 2 Smooth Muscle Cell Growth Medium (Lonza, Catalog #: CC-3182) and passaged every three days.

2.12.3. Primary peritoneal macrophages (PMs) [51]

7, 8-week-old C57BL/6J male mice were injected with 1 ml 5% (w/v) thioglycolate (Becton Dickinson, 211716) peritoneally. 72 h later, PMs were isolated from the peritoneal cavity by washing with cold PBS three times. Then, PMs were centrifuged at 1000 rpm for 5 min, and red blood cells (RBCs) were lysed by RBC lysis buffer (8.02 g/L ammonium chloride [Sigma, A9434], 0.84 g/L sodium bicarbonate [Sigma, S5761] and 0.37 g/L Ethylenediaminetetraacetic acid [Sigma, E9884] in water) for 5 min at room temperature. After that, PMs were washed with PBS twice and then plated at 10^6/ml in DMEM (Gibco, 11995-065) with 10% (v/v) fetal bovine serum (FBS) (Gibco, 10438-026), 100 U/ml penicillin (Gibco, 15140-122), 100 μg/ml streptomycin (Gibco, 15140-122). Experiments were performed at least 72 h after PMs being plated to let inflammation down.

2.12.4. THP-1-derived macrophages [51]

THP-1 cells were obtained from the American Type Culture Collection (ATCC) (ATCC, Cat# TIB-202, RRID:CVCL_0006) and kept in RPMI Medium 1640 (Gibco, 11875-093) with 10% (v/v) FBS, 100 U/ml penicillin, 100 μg/ml streptomycin, and 55 μM 2-mercaptoethanol (Gibco, 21985-023). Short-tandem repeat (STR) profiling of THP-1 cell line was performed by ATCC. Cells were replenished with 3 ml fresh medium every 2, 3 days and passaged every 6 days. THP-1-derived macrophages were differentiated in the medium containing PMA (Sigma, P1585) at a final concentration of 100 ng/ml for 72 h. The differentiated macrophages were cultured in a fresh medium without PMA for at least 72 h to let the inflammation die down before further experiments.

2.12.5. J774A.1 cells

J774A.1 cells were obtained from ATCC (ATCC, Cat# TIB-67, RRID: CVCL_0358) and passages of 6–8 were used in this study. J774A.1 cells were kept in DMEM with 10% (v/v) FBS, 100 U/ml penicillin, 100 μg/ml streptomycin, and passaged every three days.

2.12.6. HEK-Blue-hTLR4 cells

HEK-Blue-hTLR4 cells were bought from InvivoGen (InvivoGen, Catalog # hkb-htlr4) and passages of 4–7 were used in this study. Cells were kept in DMEM with 10% (v/v) FBS, 100 U/ml penicillin, 100 μg/ml streptomycin, 100 mg/ml Normocin™, and 1X HEK-Blue™ Selection. Cells were passaged every three days.

2.13. ORO staining of PMs [46,48,51]

PMs were cultured in 8-chamber cell culture slides at a density of 1×10^6 cells/ml. After treatments, cells were washed and fixed with 4% (v/v) polyformaldehyde for 15 min. After rinsing with 60% (v/v) 2-propanol (Fisher Chemical, A416-4) for 20 s, cells were stained with ORO color solution (Merck, HX7061219) for 10 min at room temperature. Next, cells were rinsed with 60% 2-propanol for 30 s, followed by distilled water for 20 s. To counterstain nucleus, cells were rinsed with hematoxylin solution (Thermo Scientific, 72511) for 10 s and then washed with running water for three minutes. Lastly, cells were mounted by an aqueous mounting agent (Merck, HC840450) and imaged freshly under the microscope.

2.14. Cell lipid extraction and quantification

Chloroform: Isopropanol: NP-40 (v:v:v = 7:11:0.1) mixture was used to extract lipids. Briefly, cells were washed with cold PBS before harvest. Add 1ml Chloroform: Isopropanol: NP-40 mix to each well and let stand for 5 min for full extraction. Transfer the lipid extract to a clean EP tube and spin the extract 5−10 min at 15,000 g. Transfer all of the liquid to a new tube, avoiding the pellet. Air-dry the extraction at 37 °C overnight. Dissolve the dried lipids with 1 ml ethanol and vortex completely. Total cholesterol and free cholesterol were detected using the Cholesterol Fluorometric Assay Kit (Cayman, 10007640). Cholesterol esters were calculated by subtracting free cholesterol from total cholesterol.

2.15. Western blot analysis

Cell protein was lysed by RIPA with proteinase inhibitors and phosphate inhibitors. Proteins were isolated in 10% SDS-PAGE and transferred to 0.45 μm nitrocellulose membranes. After blocked in 5% non-fat dry milk (LabScientific, M0841) at room temperature for one hour, membranes were firstly incubated with the primary antibodies against phosphorylated proteins listed below overnight at 4 °C and imaged after incubated with secondary antibodies. Membranes were then stripped with stripping buffer (25 mM glycine [Sigma, G7126], 1% [v/v] SDS, pH=2.0) at 100 °C for 30 min, re-blocked and incubated with primary antibodies against total proteins and β-Actin for two hours at room temperature, followed by incubation with secondary antibodies. Primary antibodies used for phosphorylated proteins: Phospho-NF-κB p65 (Ser536) (93H1) Rabbit mAb (Cell Signaling Technology, 3033, RRID:AB_331284, 1:1000) and Phospho-IκBα (Ser32) (14D4) Rabbit mAb (Cell Signaling Technology, 2859, RRID:AB_561111, 1:1000). Primary antibodies used for total proteins: NF-κB p65 and (D14E12) XP® Rabbit mAb (Cell Signaling Technology, 8242, RRID:AB_10859369, 1:1000), IκBα (L35A5) Mouse mAb (Amino-terminal Antigen) (Cell Signaling Technology, 4814, RRID: AB_390781, 1:1000), and β-Actin Antibody (Rabbit) (Cell Signaling Technology, 4967, RRID:AB_330288, 1:500). Secondary antibodies used: IRDye® 800CW Donkey anti-Rabbit IgG Secondary Antibody (LI-COR, 926-32213, RRID:AB_621848), IRDye® 680RD Donkey anti-Rabbit IgG Secondary Antibody (LI-COR, 926-68073, RRID: AB_10954442), IRDye® 800CW Donkey anti-Mouse IgG Secondary Antibody (LI-COR, 926-32212, RRID:AB_621847), and IRDye® 680RD Donkey anti-Mouse IgG Secondary Antibody (LI-COR, 926-68072, RRID:AB_10953628) in 1:5000.

2.16. Cell viability detection

Cell viability was detected using Cell Counting Kit-8 (Sigma, 96992). Briefly, cells were plated in 96-well plates (5000 cells/well) and pre-incubated overnight in a humidified incubator with 5% CO_2 at 37 °C. Cells were then incubated with 100 μl medium (as control) or miNano or HPBCD at different concentrations for 24 h in the incubator. To detect cell viability, 10 μl of CCK-8 solution was added to each well, and absorbance at 450 nm was measured using a microplate reader (Promega, GloMax Discover System).

2.17. OxLDL preparation

EDTA-free LDL (LEE Biosolutions, 360-10-0.5) was diluted in PBS to make a final concentration at 1 mg/ml. 30 μl freshly made 1 mM CuSO4 (FisherChemicals, C493-500) was added to 1ml 1mg/ml LDL, and the mix was put on an orbit shaker at 37 °C for 4 h protected from light. Reaction was stopped by adding 1% (w/v) EDTA (Sigma, E9884). After that, oxLDL was dialyzed using a dialysis device with 10K MWCO (Thermo Scientific, 88404) and stored at 4 °C for no more than one week before use. The oxidation of LDL was measured by TBARS Assay Kit (Cayman, 10009055) as about 80 nmol MDA/mg LDL protein.

2.18. Detection of membrane TLR4 activation

Before the test, HEK-Blue-hTLR4 cells were 50−80% confluent. 20 μl of negative control (PBS), positive control (20 ng/ml LPS), or tested solution per well was added to a flat-bottom 96-well plate. HEK-Blue-hTLR4 cells were resuspended in HEK-Blue Detection medium at around 140,000 cells/ml. 180 μl of the cell suspension was added per well immediately. Cells were incubated at 37 °C in 5% CO_2 for 9 h, and hTLR4 activation was detected by absorbance at 620−655 nm using a microplate reader.

2.19. Human samples

The human samples used in this study were collected from the patients who were underwent open surgical repair of aortic aneurysm with the Institutional Review Board approval (Hum0077616) from the Cardiovascular Health Improvement Project (CHIP) and Institutional Review Boards of the University of Michigan Medical School. We selected and prepared sections for observing CCs in the ascending aortas with or without atherosclerotic lesions.

2.19.1. ORO staining of human aortic arteries [46,48,51]

The atherosclerosis-bearing aortas from human ascending aortic aneurysm lesions were frozenly sectioned at 7 um after fixing. ORO staining was performed as described above. The aorta area without atherosclerotic plaques was used as a control.

2.20. Removing CCs in human atherosclerotic plaques

The atherosclerosis-bearing aortas from human ascending aortic aneurysm lesions were frozenly sectioned at 7 um after fixing. The same volume of PBS, miNano, or HPBCD diluted in pooled serum was added to sections and incubated at 37 °C for 24 h, avoiding light. Adjacent sections of each group without any treatment were used as a baseline. CCs were detected under polarized light, and quantification was analyzed by Image J software.

2.21. Cell line and antibody validation

Cell lines used in the current study were validated by the institute, and STR profiling of the cell lines is listed in Supplementary materials 2. Cell lines are free of mycoplasma contamination. All antibodies used in the current study are commonly used antibodies, verified by the institute, and RRID tags are indicated. Relevant references for application of the antibodies are listed in Table S3.

2.22. Statistics

Statistical analysis was performed using GraphPad Prism 9.0. Normality was tested for all data using D'Agostino & Pearson test or Anderson-Darling test. Variance equality was tested for all data using Brown-Forsythe test. Data are presented as mean ± SD or median (IQR). Outliers were detected and excluded by ROUT method (Q = 1%) when necessary. When comparing the difference of one variable among more than two groups, in cases of normal distribution and equal variance, one-way analysis of variance (ANOVA) followed by Dunnett's multiple comparisons test, Sidak's multiple comparisons test, or Tukey's multiple comparisons test was performed; Otherwise, Kruskal-Wallis test followed by Dunn's multiple comparisons test were used. Repeated measures ANOVA followed by Tukey's multiple comparisons test was performed to compare the difference of body weight change along with time. A p value < 0.05 was considered statistically significant ($^{*}p < 0.05$, $^{**}p < 0.01$, $^{***}p < 0.001$). For *in vitro*

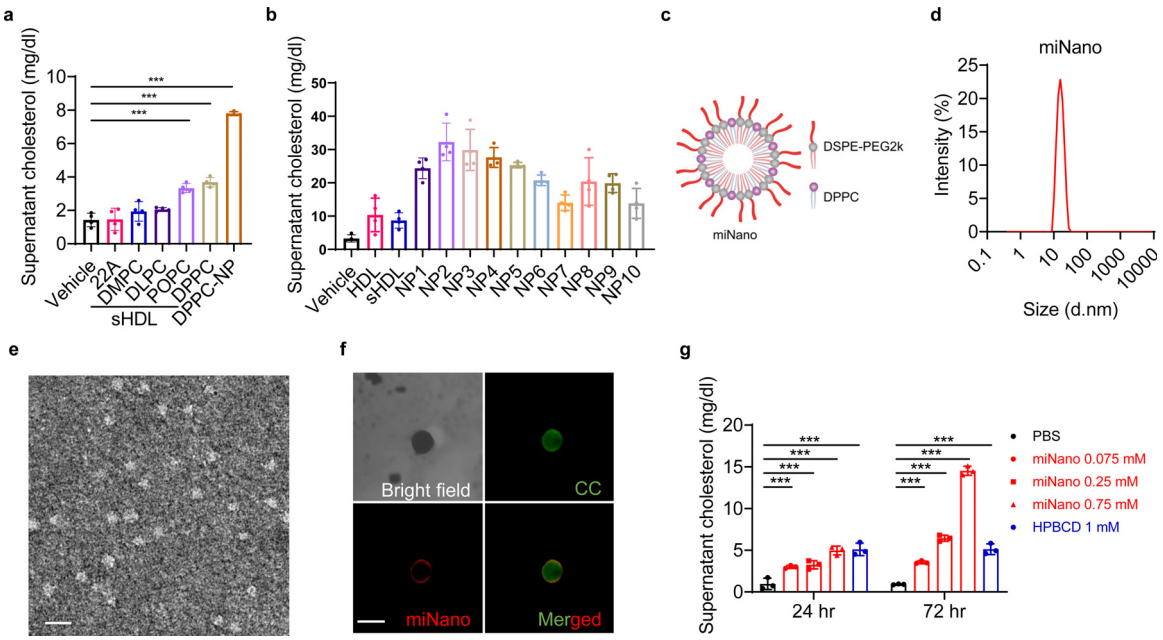

Fig. 1. Characterization of miNano. (**a**) 200 μg/well CCs were incubated with indicated conditions: vehicle, 100 μg/ml 22A, 100 μg/ml sHDL composed of 22A and indicated lipid components (DMPC, DLPC, POPC, or DPPC), or 50 μM nanoparticles constituted with DPPC and DSPE-PEG2k in a 1:1 ratio without 22A. Supernatant cholesterol level was measured (n = 4). (**b**) 200 μg/well CCs were incubated with vehicle, 300 μg/ml native HDL, 300 μg/ml sHDL composed of 22A and DPPC, or 0.75 mM NPs (NP1-NP10) constituted with DSPE-PEG2k/DSPE-PEG5k and/or DPPC in different molar ratios without 22A. The concentration of sHDL was indicated as 22A peptide concentration, and NPs were given at the same molar concentration of lipids as sHDL. Supernatant cholesterol level was measured (n = 4). (**c**) Schematic diagram of miNano (NP2).(**d**) DLS analysis, and (**e**) a representative image of miNano by TEM. (**f**) Representative images by confocal microscope after incubating NBD-CCs (green) with 0.15 mM Rhodamine PE-miNano (red) for 1 h. (**g**) 200 μg/well CCs were incubated with vehicle, miNano at indicated concentrations, or 1 mM HPBCD. Supernatant cholesterol was detected at 24 h or 72 h (n = 6). Results are representatives of at least three independent experiments. Data are mean ± SD. Statistical difference was determined by ordinary one-way ANOVA and followed by Dunnett's multiple comparisons test. $^{***}p < 0.001$. Scale bars: (**e**) 20 nm, (**f**) 25 μm. Abbreviations: DMPC, 1,2-dimyristoyl-sn-glycero-3-phosphocholine, DLPC, 1,2-dilauroyl-sn-glycero-3-phosphocholine, POPC, 1-palmitoyl-2-oleoyl-glycero-3-phosphocholine, DPPC, 1,2-dipalmitoyl-sn-glycero-3-phosphocholine, DSPE-PEG2k, 1,2-distearoyl-sn-glycero-3-phosphoethanolamine-N-[amino(polyethylene glycol)-2000].

studies, results presented are representative results of three replicates.

2.23. Study approval

All animal procedures were approved by the Institutional Animal Care and Use Committee of the University of Michigan (PRO00008239) and performed according to the institutional guidelines. The human surgery tissues were frozen in liquid nitrogen and stored in the CHIP core in the Department of Cardiac Surgery at the University of Michigan. The consent was signed by the patient before the surgery. The tissue collection was approved with the Institutional Review Board approval (Hum0077616) from the Human Research Protection Program and Institutional Review Boards of the University of Michigan Medical School.

2.24. Role of funding source

Funders providing financial support for this study do not participate in study design, data collection, data analyses, interpretation, or writing of report.

3. Results

3.1. Generation of HDL-like and phospholipid-based miNano particles

The phospholipid components determine cholesterol efflux and anti-inflammatory properties of endogenous HDL and sHDL particles [41]. Considering the critical role of CCs in atherosclerosis, we first evaluated the CC-dissolving capacity of sHDL particles composed of different phospholipids and 22A, an ApoA-I mimetic peptide designed for sHDL clinical application [46,47]. Unexpectedly, 22A itself did not dissolve CCs (Fig. 1a), indicating that the lipid components of sHDL particles execute this CC-dissolving function. Among different sHDLs, we found that sHDL particles composed of 1,2-dipalmitoyl-sn-glycero-3-phosphocholine (DPPC) and 22A had the highest CC-dissolving ability (Fig. 1a). As PEGylation of NPs improves the *in vivo* stability and prolongs the circulation [52], we combined DPPC with 1,2-distearoyl-sn-glycero-3-phosphoethanolamine-N-[amino (polyethylene glycol)-2000] (DSPE-PEG2k) or DSPE-PEG5k to obtain amphipathic NPs with hydrophobic fatty acid tails facing the inside, making them suitable for carrying hydrophobic molecules such as cholesterol. Next, we optimized NPs (NP1-NP10) using DPPC and DSPE-PEG2k or DSPE-PEG5k at different molar ratios (Table S1). All the NPs dissolved CCs more efficiently than native HDL or sHDL at the same molar concentration of lipids (Fig. 1b). Among the NPs, NP2 exerted the best CC-dissolution as indicated by a threefold increase compared to HDL or sHDL group. NP2 was then renamed as miNano, which was composed of DPPC and DSPE-PEG2K at a 1:2 molar ratio (Fig. 1c). miNano particles were highly homogeneous with an average diameter of 15·8 ± 0·2 nm and a polydispersity index (PDI) of 0·10 ± 0·04 analyzed by DLS and TEM imaging (Fig. 1d and e).

To study the interaction of miNano and CCs, we generated NBD-CCs using 25-NBD cholesterol (green fluorescence) and miNano labeled with Rhodamine phycoerythrin (Rhodamine PE-miNano, in red fluorescence, with a similar diameter to miNano particles as shown in Fig. S1). We visualized the direct binding of miNano to CCs under a confocal microscope (Fig. 1f). The CC-dissolution test revealed that miNano particles dissolved CCs more robustly than HPBCD (Fig. 1g), which is known to dissolve CC and is widely used to improve the aqueous solubility of various compounds. Thus, we generated a novel phospholipid-based NP, miNano, which functions as better cholesterol acceptors and has a more robust CC-dissolving capability than HDL particles and HPBCD.

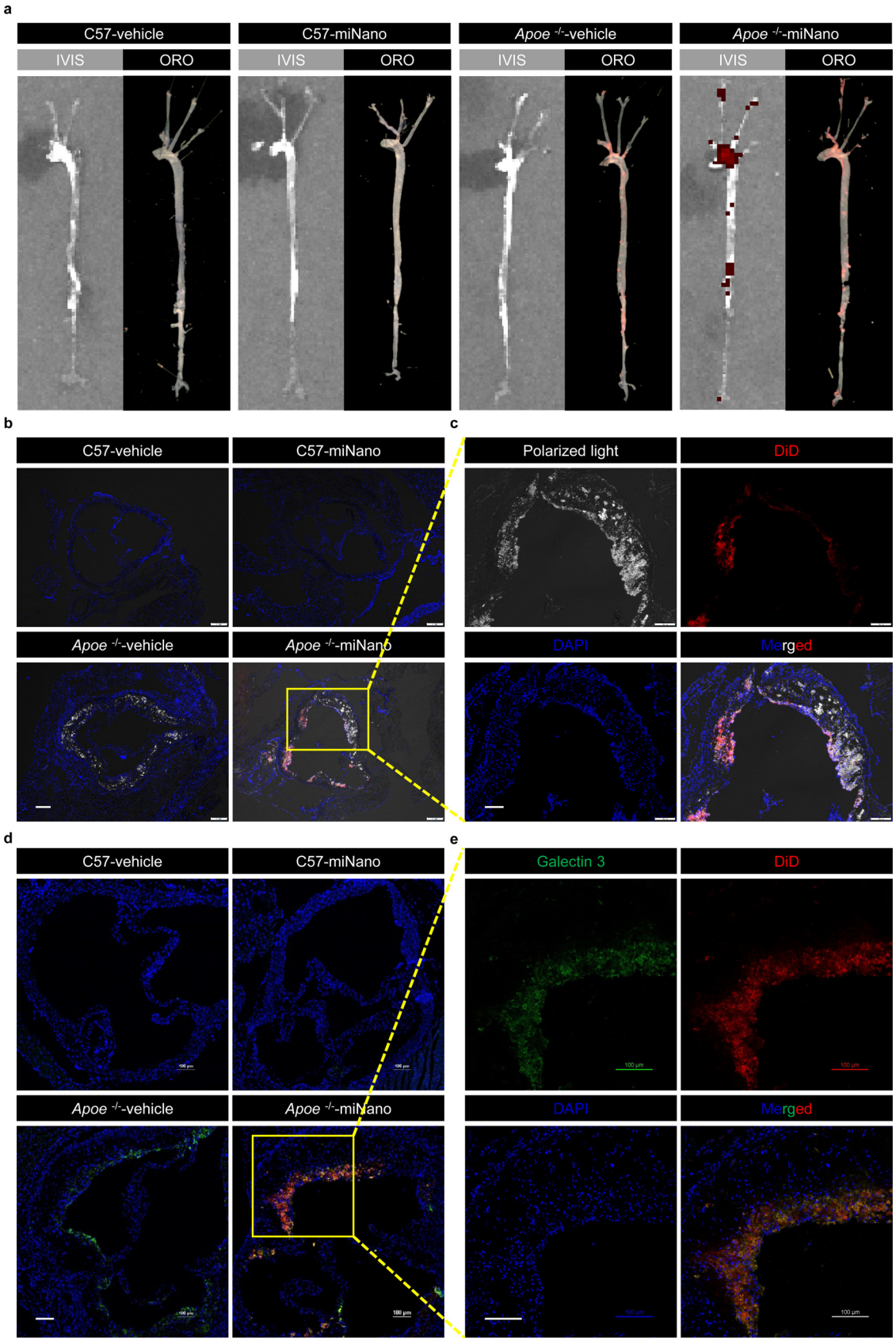

Fig. 2. miNano targets CCs and macrophages in atherosclerotic plaques *in vivo*. *Apoe*-deficient mice fed on a western diet or C57BL/6J mice fed on a standard laboratory diet for 12 weeks were given one dose of vehicle or 250 mg/kg DiD-miNano via tail vein ($n = 4$). 24 h later, aortas were collected for (**a**) imaging DiD by IVIS and lipids by ORO stain; Aortic sinus was sectioned for (**b** and **c**) visualizing CCs under polarized light and (**d** and **e**) staining macrophages by galectin 3 antibody. (**b**) Representative merged images of DAPI-stained aortic sinus slides under a fluorescent microscope. (**c**) Magnified images from the yellow box in (**b**) under separated channels. (**d**) Representative merged images of DAPI- and galectin 3-stained aortic sinus slides under a confocal microscope. (**e**) Magnified images from the yellow box in (**d**) under separated channels. (**b**–**e**) DiD-miNano was detected by Cy5 fluorescent signal. Scale bars: (**b**) 200 μm, (**c**–**e**) 100 μm.

3.2. miNano accumulates in atherosclerotic plaques

We asked whether miNano could target atherosclerotic plaques *in vivo*. A far-red fluorescent dye (DiD) labeled miNano (DiD-miNano) was administrated *via* intravenous (IV) injection into atheroma-bearing *Apoe*-deficient mice and control C57BL/6J mice. 24 h after injection, isolated aorta trees were imaged for DiD-miNano distribution by *in vivo* imaging system (IVIS) and then stained with Oil Red O (ORO) for labeling atherosclerotic plaques. We found that DiD-fluorescent distribution coincided with atherosclerotic plaques stained by ORO in aortas from *Apoe*-deficient mice, while DiD and ORO staining were almost undetectable in aortas from C57BL/6J mice (Fig. 2a), indicating that miNano enters and accumulates in the atherosclerotic plaques but not the normal aorta wall *in vivo*.

Then the aortic sinus was sectioned to examine CCs under a polarized light microscope and macrophages using an antibody against galectin 3/Mac2, a widely used macrophage marker in mouse studies. There were substantial CCs in atherosclerotic plaques from *Apoe*-deficient mice (Fig. 2b), where DiD-miNano co-localized with CCs (Fig. 2c). Significant macrophages also accumulated and co-localized with DiD-miNano in the plaques of *Apoe*-deficient mice (Fig. 2d and e). In contrast, CCs, macrophages, and DiD-miNano were nearly unobservable in sections of the aortic sinus from C57BL/6J mice (Fig. 2b and d). Biodistribution imaging revealed that miNano mainly accumulated in the liver with fewer accumulations in the spleen, bone marrow, lung, small intestine, and kidney (Fig. S2). These findings demonstrate that miNano accumulates in atherosclerotic plagues, co-localizing with CCs and macrophages.

3.3. miNano inhibits atherosclerosis in Ldlr-deficient mice independent of lipid profile

To determine the therapeutic potential of miNano, we tested if miNano can ameliorate atherosclerosis *in vivo*. In a pilot study, *Apoe*-deficient mice were fed with a 12-week western diet to develop atherosclerosis, and then the atheroma-bearing mice were grouped randomly to be sacrificed as the baseline or treated with vehicle, miNano, or HPBCD *via* tail vein injection twice a week for additional 6 weeks. At the beginning of treatment, we changed the western diet to a standard laboratory diet to mimic the fact that individuals are recommended to consume a healthier diet after diagnosed with coronary artery disease in the clinic (Fig. S3a). miNano treatment significantly decreased the aortic plaque area in both male and female mice, but HPBCD only reduced aortic plaque area in male mice (Fig. S3b–d).

Due to loss-of-function mutations in *LDLR*, lots of patients with familial hypercholesteremia suffer from resistance to statins and PCSK9 inhibitors. To further investigate if miNano would also ameliorate atherosclerosis by mechanisms escaping LDLR, we evaluated the efficacy of miNano in Ldlr-deficient mice, mimicking FH patients. *Ldlr*-deficient micebearing atheroma were grouped and treated in the same way of Apoe-deficient mice as described above (Fig. 3a). Although none of the treatments regressed atherosclerotic plaques compared with the baseline, the administration of miNano dramatically decreased the aortic plaque area (Fig. 3b–d), aortic sinus plaque CC area, and macrophage infiltration compared to vehicle both in male and female mice (Figs. 3e, f–i, S4). Besides, miNano significantly increased plaque stability as indicated by diminished necrotic core and higher collagen content in plaques determined by Masson's trichrome stain (Figs. S5, 7j–m). However, except for an increase in plaque collagen area in male mice (Fig. 3i), HPBCD showed a minimal effect in improving the atherosclerosis parameters in male and female *Ldlr*-deficient mice. miNano administration exerted no effect on plasma TNFα and IL-6 levels compared to vehicle both in male and female mice, which may be because that the general circulating TNFα and IL-6 levels are very low in mice (Fig. S6).

To determine if miNano benefits atherosclerosis by ameliorating blood lipids, we measured plasma lipid and lipoprotein profile (Fig. S7a–h). We observed that plasma triglyceride and HDL levels showed no difference among the three treated groups. However, plasma TC and LDL levels were elevated in miNano-treated male and female mice compared to vehicle control mice. We assumed that the increased plasma TC level was transient due to cholesterol mobilization by CC dissolution. To prove this, we fed *Ldlr*-deficient mice with western diet for 2 weeks and treated them with five doses of miNano as indicated in Fig. S7i. To see the plasma cholesterol changes, we collected the plasma and measured the plasma cholesterol at 0 h, 24 h, and 72 h after the last dose of miNano. We found that miNano induced a transient increase in plasma TC 24 h after the injection, but then the TC level fell back to baseline after 72 h (Fig. S7j).

To further investigate if the mobilized cholesterol can be excreted outside the body, we measured the fecal bile acids from mice in Fig. 3a. We found that miNano promoted excretion of multiple bile acids (Fig. S7k), implying that the mobilized cholesterol would finally be eliminated out of the body. Altogether, the above results indicate that miNano slowed down the development of atherosclerosis independent of ameliorating lipid profile, but instead most possibly by decreasing CC burden and macrophage infiltration in *Ldlr*-deficient mice.

3.4. Favorable safety profiles of miNano in Ldlr-deficient mice

During the 6-week treatment period, as indicated in Fig. 3a, all animals appeared healthy with normal activity, and no significant body weight change was noted in both male and female mice (Fig. 4a, b). At the sacrifice, macroscopic examination of organs including heart, liver, kidney, spleen, lung, intestine, and brain tissue showed no signs of necrosis, hyperplasia, or inflammation after a 6-week administration of miNano, as compared to that of control mice. Administration of miNano did not induce liver and kidney damage, as indicated by the alanine aminotransferase (ALT), aspartate aminotransferase (AST), albumin (ALB), total bilirubin (TBil), and alkaline phosphatase (ALP), creatinine (CREA), and blood urea nitrogen (BUN) levels (Fig. 4c–i). miNano even reduced plasma CREA level for unclear mechanism. Besides, no obvious pathological signs were observed in different tissue sections from miNano- or HPBCD-treated mice compared to vehicle-treated mice (Figs. 4j, S8). To further evaluate the safety profile of miNano, two cohorts of mice were treated with five doses of either vehicle or miNano, after which blood was collected for complete blood count analysis. The results are shown in Table S4. We found that miNano did not influence blood cells count and the related indexes. In summary, the above findings illuminated that miNano ameliorates atherosclerosis development in *Ldlr*-deficient mice with a favorable safety profile.

3.5. miNano is biocompatible to multipme vascular cells

To investigate if miNano is cytotoxic to vascular cells, we tested the effect of miNano on the viability of PMs, primary human coronary artery endothelial cells and primary human smooth muscle cells (Fig. S9). miNano did not influence cell viability as high as 750 uM.

3.6. miNano prevents foam cell formation in vitro

Since we observed decreased CC and macrophage areas in plaques of mice treated with miNano, we asked whether miNano has any effects on foam cell formation. Mouse PMs were incubated with oxidized-LDL (oxLDL) to induce foam cell formation indicated by intracellular lipid accumulation by ORO stain. miNano treatment dramatically decreased lipid accumulation, and HPBCD showed a beneficial but weaker effect (Fig. 5a), which was then confirmed by intracellular cholesterol ester, total cholesterol, and free cholesterol levels (Fig. 5b–d). Besides, miNano treatment inhibited oxLDL-

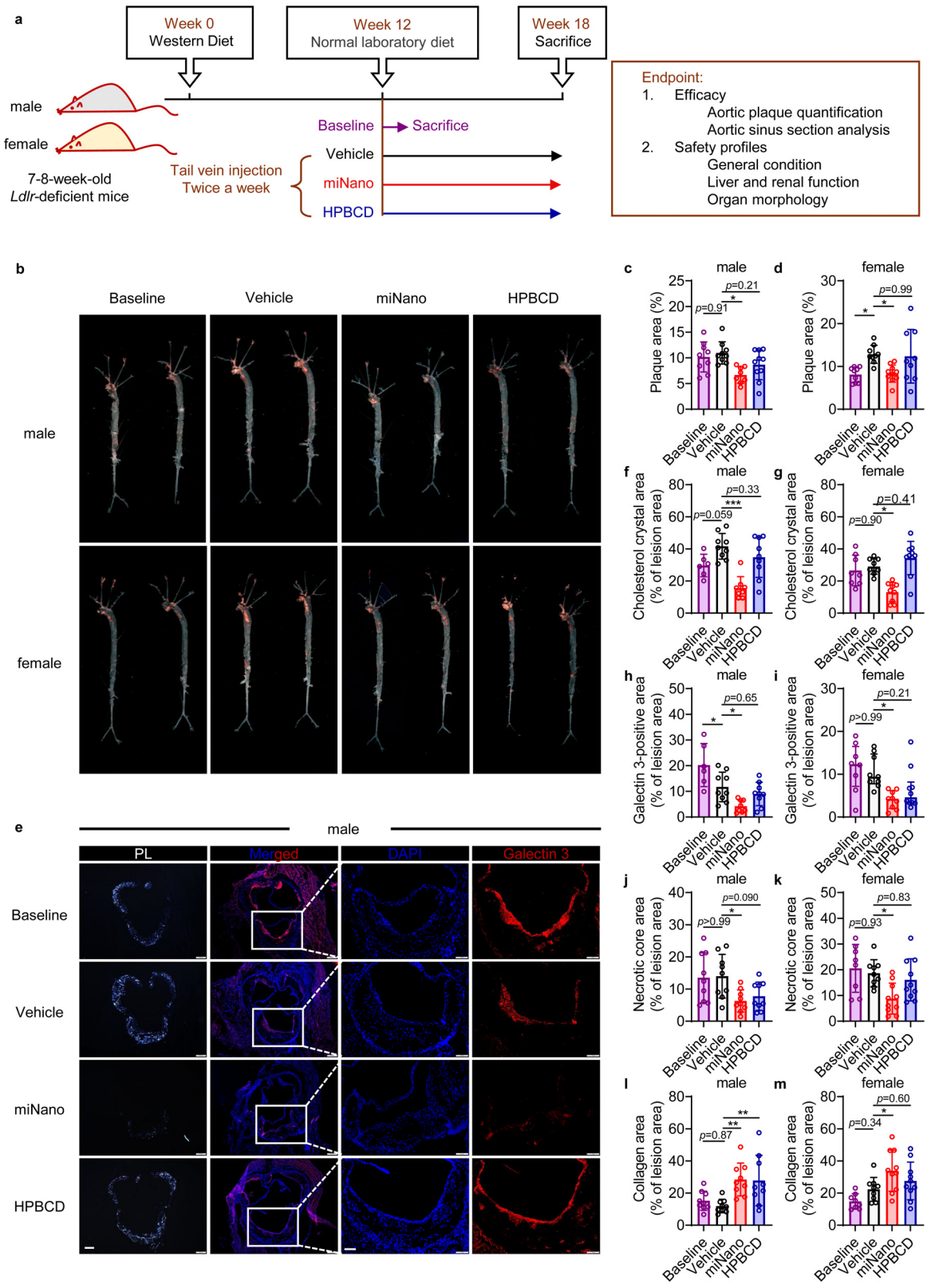

Fig. 3. miNano inhibits atherosclerosis in *Ldlr*-deficient mice. (**a**) Schematic diagram of treatment. 7, 8-week-old male and female *Ldlr*-deficient mice were challenged with a western diet for 12 weeks to establish atherosclerosis. Mice were then fed on a normal laboratory diet and randomized to either be sacrificed as a baseline or treated by vehicle, 250 mg/kg miNano, or 400 mg/kg HPBCD twice a week via tail vein injection for 6 weeks. Mice were sacrificed 48 h after the last injection at the end of the 18th week. Aortas were isolated for ORO staining, and aortic sinus was sectioned for galectin 3 staining to detect macrophages and Masson's trichrome staining to detect necrotic core and collagen content (n = 6–10). (**b**) Representative images and quantification of plaque area in (**c**) male and (**d**) female aortas stained by ORO. (**e**) Representative images and quantification of (**f, g**) CCs and (**h, i**) galectin 3-positive area in aortic sinus sections from male and female mice. Quantification of (**j, k**) necrotic core area and (**l, m**) collagen content by Masson's trichrome staining in aortic sinus sections from male and female mice. Data are mean ± SD. Statistical difference was determined by ordinary one-way ANOVA and followed by Sidak's multiple comparisons test or Tukey's multiple comparisons test. * $p < 0.05$, ** $p < 0.01$, *** $p < 0.001$. Scale bars: the left two panels of (**e**) 200 μm, the right two panels of (**e**) 100 μm. Abbreviation: PL, polarized light.

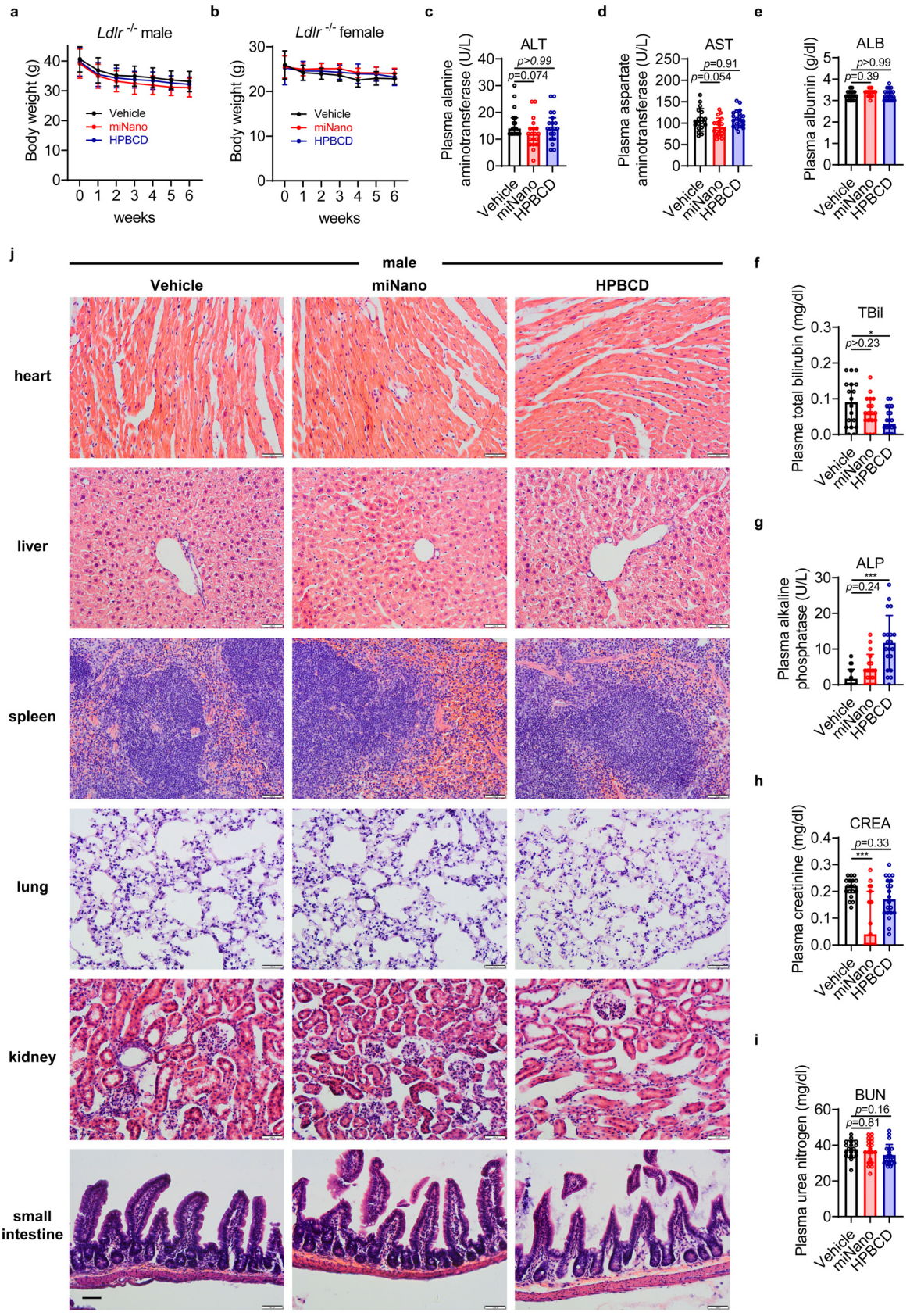

Fig. 4. Favorable safety profiles of miNano administration in *Ldlr*-deficient mice. Mice were treated and sacrificed as described in Fig. 3a. Bodyweight of (**a**) male and (**b**) female mice during the treatment period (n = 6–10). The plasma (**c**) alanine transaminase, (**d**) aspartate aminotransferase, (**e**) albumin, (**f**) total bilirubin, (**g**) alkaline phosphatase, (**h**) creatine, and (**i**) blood urea nitrogen of both male and female mice (n = 13–16). (**j**) H&E staining of heart, liver, spleen, lung, kidney, and small intestine. Data are mean ± SD or median with IQR. Outliers were detected and excluded by ROUT method (Q = 1%). (**a, b**) Statistical difference was determined by repeated-measures ANOVA followed by Tukey's multiple comparisons test. (**c**–**i**) Statistical difference was determined by ordinary one-way ANOVA and followed by Dunnett's multiple comparisons test, or by Kruskal-Wallis test followed by Dunn's multiple comparisons test. $^{*}p < 0.05$, $^{***}p < 0.001$. Scale bars: 100 μm. Abbreviations: ALT, alanine transaminase; AST, aspartate aminotransferase; ALB, albumin; TBil, total bilirubin; ALP, alkaline phosphatase; CREA, creatine; BUN, blood urea nitrogen.

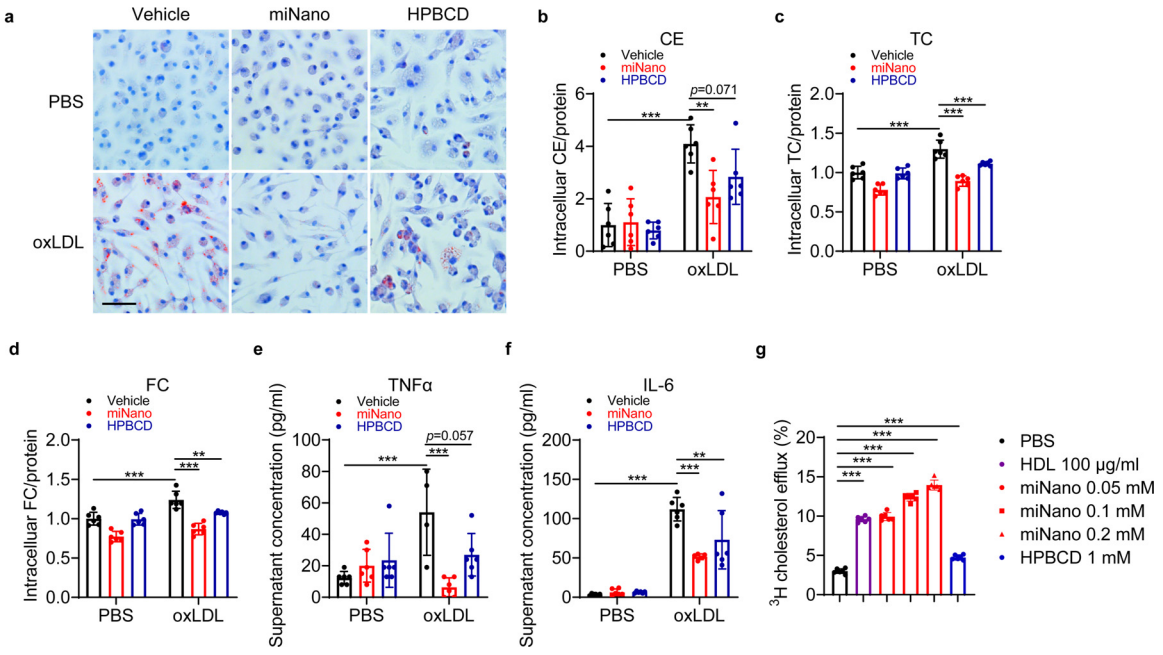

Fig. 5. miNano prevents foam cell formation. PMs were treated with either vehicle or 50 μg/ml oxLDL for 24 h. At the same time, cells were treated with PBS, 0.15 mM miNano, or 1 mM HPBCD. (**a**) Representative images of ORO staining. Quantification of (**b**) cholesterol ester, (**c**) total cholesterol, and (**d**) free cholesterol in PMs (n = 6). Determination of cell culture supernatant (**e**) TNFα and (**f**) IL-6 levels by ELISA (n = 6). (**g**) Cholesterol efflux capacity in J774A.1 cells by PBS, 100 μg/ml HDL, 0.05, 0.1, or 0.2 mM miNano, or 1 mM HPBCD (n = 6). Results are representatives of at least three independent experiments. Data are mean ± SD. Outliers were detected and excluded by ROUT method (Q=1%). Statistical difference was determined by ordinary one-way ANOVA and followed by Sidak's multiple comparisons test or Tukey's multiple comparisons test. $^{**}p < 0.01$, $^{***}p < 0.001$. Scale bar: 50 μm. Abbreviations: CE, cholesterol ester; TC, total cholesterol; FC, free cholesterol.

induced inflammatory responses in PMs, as implied by decreased supernatant TNFα and IL-6 levels (Fig. 5e, f) and decreased *Tnf, Il1b, and Nlrp3* transcription (Fig. S10). Since sHDLs function as cholesterol acceptors to mediate cholesterol efflux from macrophages, we speculated that miNano might also promote cholesterol efflux from macrophages, thus reducing foam cell formation and inflammation. Indeed, we found that miNano induced cholesterol efflux dose-dependently in J774A.1 cells, a mouse macrophage cell line, while HPBCD showed a weaker effect (Fig. 5g). The above results demonstrated that miNano particles prevented foam cell formation and inflammation at least partially via enhancing cholesterol efflux.

3.7. miNano reduces inflammatory responses induced by CCs in macrophages

Besides oxLDL, CCs are also highly pro-inflammatory in atherosclerotic plaques [15,53]. To further investigate if miNano inhibits CC-induced inflammation in macrophages, we treated THP-1-derived macrophages with vehicle, miNano, or HPBCD in the presence or absence of CCs. As expected, CCs induced significant inflammatory responses in macrophages [15], while miNano treatment inhibited the CC-triggered release of TNFα, IL-6, IL-1β, and CCL2 (Fig. 6a–d) as well as the transcription of these cytokines (Fig. S11). Surprisingly, HPBCD seemed to aggravate inflammatory response in macrophages (Figs. 6c, S11a, S11c), which may be caused by the HPBCD-cholesterol mixture-mediated cholesterol loading [54].

Considering that membrane cholesterol-rich domains modulate Toll-like receptors (TLRs)-dependent inflammatory pathways, we asked whether miNano influenced the TLR4-NF-κB pathway as miNano decreased the transcription of several inflammatory cytokines. We used HEK-Blue-hTLR4 cells, a commercially available cell line designed to investigate the stimulation of human TLR4 by monitoring NF-kB activation. We found that miNano inhibited human TLR4 activation stimulated by LPS in a dose-dependent manner, while HPBCD displayed little effect (Fig. 6e). Nuclear factor-κB (NF-κB) is a critical transcription factor in inflammatory responses, and NF-κB phosphorylation is required for the induction of its target genes. IκBα is the endogenous NF-κB inhibitor protein, and phosphorylation of IκBα leads to its degradation in the proteasome [55]. Western blot results showed that miNano dramatically reduced LPS-induced phosphorylation of p65 and IκBα in THP-1-derived macrophages (Fig. 6f–i), indicating that miNano inhibited the transcription of NF-κB target genes by suppressing the activation of NF-κB and degradation of IκBα, while HPBCD did not show any beneficial effect. Thus, those results demonstrated that besides dissolving CC directly, miNano also inhibited inflammatory responses by suppressing the TLR4/NF-κB signaling pathway in macrophages.

3.8. miNano dissolves CCs in human atherosclerotic plaques

To further investigate if miNano can dissolve CCs in human atherosclerotic plaques, we sectioned the ascending aortas with atherosclerotic lesions from patients who underwent open surgical repair of aortic aneurysms (Fig. S12). The crystal signal in the plaques was soluble in xylene, an organic solvent, but resistant to hydrochloric acid (HCl), a decalcifying agent, proving that the crystals we observed under a polarized light microscope are CCs, not calcium crystals (Fig. S13). To better mimic the application of miNano in CAD patients, we diluted miNano or HPBCD using pooled serum from *Apoe*-deficient mice with LDL-cholesterol levels at around 500 mg/dl and triglycerides at about 100 mg/dl, similar to that in familial hypercholesteremia patients [56]. After 24 h incubation with the miNano-serum mixture, CCs in human atherosclerotic plaques were dissolved in a dose-dependent way (Fig. 7a, b). HPBCD-serum mixture tended to dissolve CCs but did not reach statistical significance. These results potentiate the application of miNano as a novel strategy to treat atherosclerosis in the clinic by removing CCs in plaques.

4. Discussion

In the current study, we developed miNano, a novel HDL-mimicking phospholipid-based nanomedicine that inhibited atherosclerosis

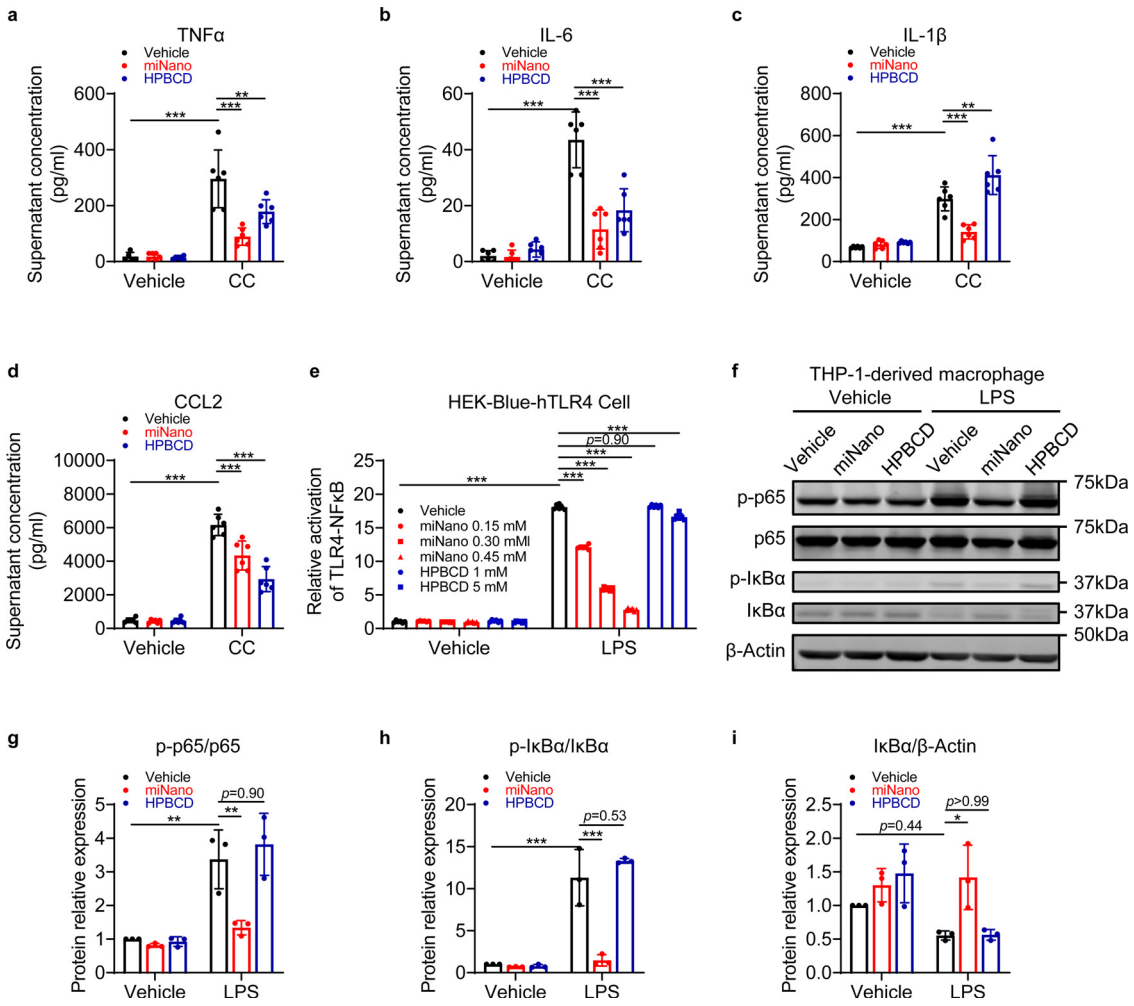

Fig. 6. miNano reduces macrophage inflammation via inhibiting TLR4-NF-κB pathway. (**a**-**d**) THP-1-derived macrophages were treated with vehicle, 0.15 mM miNano, or 1 mM HPBCD in the absence or presence of 300 μg/ml CCs for 24 h. Cell culture supernatant was collected for quantification of (**a**) TNFα, (**b**) IL-6, (**c**) IL-1β, and (**d**) CCL2 by ELISA (n = 6). (**e**) HEK-Blue-hTLR4 cell was treated with vehicle, 0.15, 0.30, or 0.45 mM miNano, or 1, 5 mM HPBCD in the absence or presence of 20 ng/ml LPS for 9 h, then human TLR4 activation was detected (n = 6). (**f**–**i**) THP-1-derived macrophages were pre-incubated with vehicle, 0.15 mM miNano, or 1 mM HPBCD for 20 min, and then either vehicle or LPS at a final concentration of 100 ng/ml was added to the medium for 15 min. Cells were harvested for western blot (n = 3). (**f**) Representative images of western blot against phosphorylated p65, p65, phosphorylated IκBα, and IκBα in THP-1-derived macrophages. Quantification of (**g**) phosphorylated p65/p65, (**h**) phosphorylated IκBα/IκBα, and (**i**) IκBα/β-Actin of western blot in THP-1-derived macrophages. Results are representatives of at least three independent experiments. Data are mean ± SD. Outliers were detected and excluded by ROUT method (Q = 1%). Statistical difference was determined by ordinary one-way ANOVA and followed by Sidak's multiple comparisons test or Tukey's multiple comparisons test. $^{*}p < 0.05$, $^{**}p < 0.01$, $^{***}p < 0.001$. Abbreviations: p-p65, phosphorylated p65; p-IκBα, phosphorylated IκBα.

development in both genders of *Ldlr*-deficient mice with favorable safety profiles by removing plaque CCs, promoting cholesterol efflux, and reducing inflammatory responses in macrophages. miNano is composed of DPPC and DSPE-PEG2k, both of which are biocompatible and FDA-approved pharmaceutical excipients. Besides, nanoparticles formulated by DSPE-PEG were reported to decrease cellular cholesterol contents [57]. Like rHDL particles [46], miNano can accumulate in atherosclerotic plaques because the average diameter (16 nm) of miNano facilitates it enter atherosclerotic plaques. Interestingly, we did not detect the accumulation of miNano in normal arterial walls of C57BL/6J mice, which may be attributed to the higher physical binding affinity of DPPC to cholesterol as excessive cholesterol accumulation is the hallmark of atherosclerosis. The increased penetration of miNano due to the impaired endothelial barrier in atherosclerotic arteries may be another mechanism. We also observed that miNano co-localized well with macrophages within plaques, implying that phagocytosis by monocyte in the circulation followed by accumulation in the plaque may be another way for miNano to enter into plaques, though the latter is less likely since the relatively small diameter of miNano prevents it from phagocytosis [58]. Like most rHDLs [59], miNano is eliminated by the liver with limited elimination by the kidney, as shown by fluorescence signal accumulation. As HPBCD is primarily distributed in the kidney [60], quick elimination after the intravenous injection may be one of the reasons causing less beneficial effects of HPBCD on atherosclerosis in this study.

Using *Ldlr*-deficient mice, we verified that miNano inhibited atherosclerosis and stabilized plaque. We did not observe atherosclerosis regression after switching the western diet to a standard laboratory diet, which may be caused by the age-related deterioration of atherosclerosis in *Ldlr*-deficient mice [61]. Administration of miNano efficiently decreased plaque burden and CC burden in both genders of *Ldlr*-deficient mice, accompanied by a similar shrink in macrophage infiltration into plaques and increased stability of plaques. Administration of HPBCD showed limited beneficial effects on atherosclerosis in this study compared to Zimmer et al.'s study [29], possibly because a relatively lower dosage of HPBCD was administrated (a total of 4.8 g/kg by IV injection in this study vs. 16 g/kg via subcutaneous injection in Zimmer et al.'s study). Actually, the impacts of HPBCD on lipid profiles and atherosclerosis vary among studies due to differences in administration methods, dosage, and animal models [62]. Besides, a prolonged half-life about 16 h (Anna S. Schwendeman,

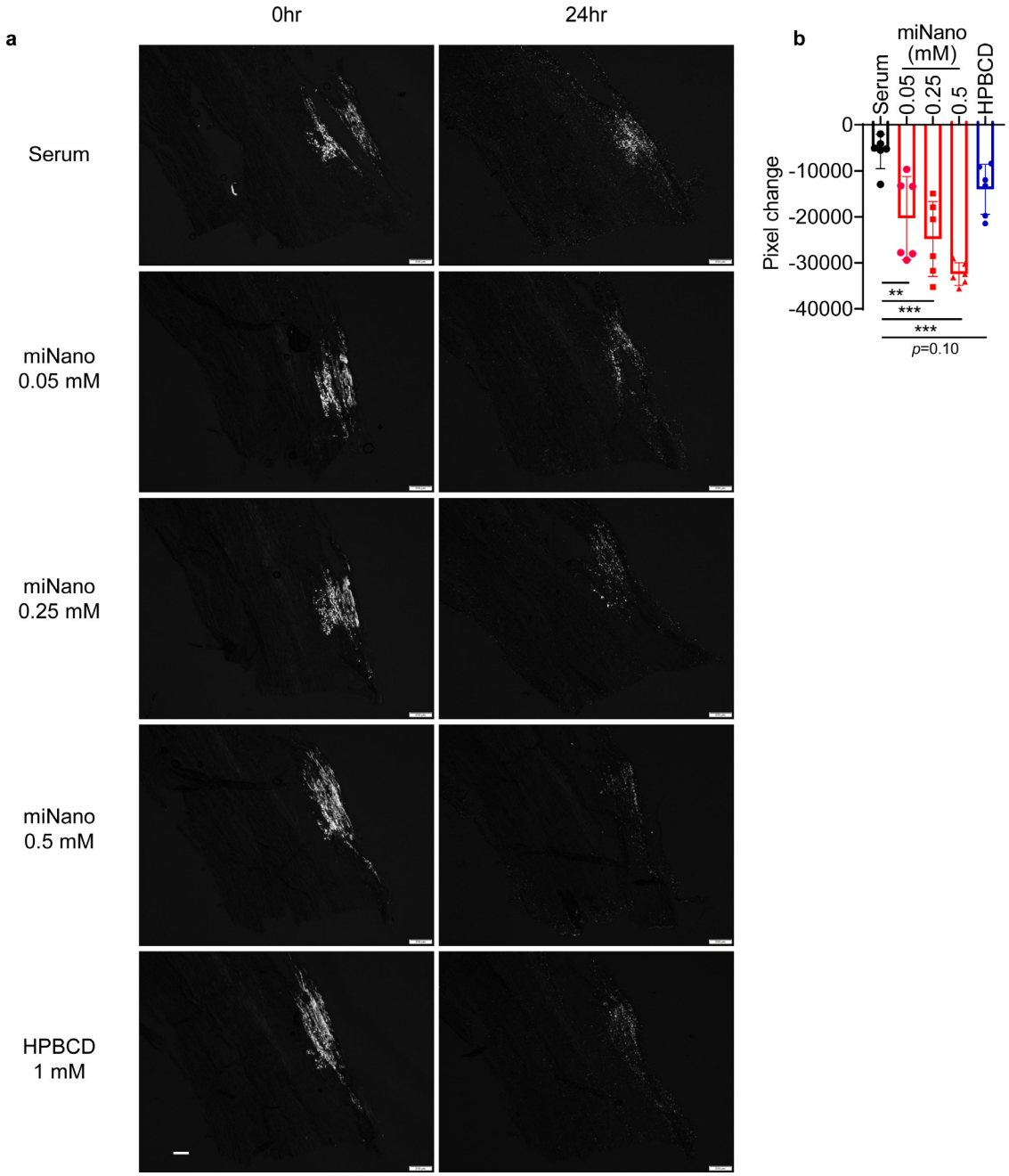

Fig. 7. miNano dissolves CCs in human atherosclerotic plaques. Sections from thoracic aortas bearing atherosclerotic plaques from thoracic arterial aneurysm patients were used. Adjacent sections were incubated with serum, serum mixed with miNano or HPBCD at indicated concentrations for 24 h under 37 °C protected from light (n = 6). Pooled serum from *Apoe*-deficient mice with a total cholesterol level being around 500 mg/dl and triglyceride being about 100 mg/dl was used to dilute miNano or HPBCD. (**a**) Representative images and (**b**) quantification of changes in CC signal under polarized light (n = 6). Data are mean ± SD. Statistical difference was determined by ordinary one-way ANOVA and followed by Dunnett's multiple comparisons test. ** $p < 0.01$, *** $p < 0.001$. Scale bar: 200 μm.

unpublished) of miNano also enables it to be more effective than the rapid elimination of HPBCD [46]. The beneficial effect of miNano in *Ldlr*-deficient mice potentiates it as a promising therapy for treating atherosclerosis in familial hypercholesteremia patients.

Traditional murine atherosclerotic models usually lack features of plaque rupture as observed in human, including thin cap fibroatheroma, intraplaque hemorrhage, vasa vasorum, and thrombosis. In the current study, we did not observe typical features of plaque rupture in *Ldlr*-deficient mice. Instead, we try to evaluate plaque stability by quantifying necrotic core and collagen area, two indexes related to human plaque vulnerability. In this way, we proved that miNano stabilized plaques. Researchers have tried to establish advanced murine models to study plaque vulnerability and rupture [63–65], which, however, is hard to be widely applied due to technique issues. In the future, it's necessary to evaluate the effects of miNano on plaque stability in more proper models.

Foam cell formation, which represents dysfunctional macrophages, plays an essential role in all atherosclerosis stages. HPBCD has been proved to reduced foam cell formation at extremely high dose (40–80 mM) [66]. Here, we showed that miNano promoted macrophage cholesterol efflux and prevented foam cell formation better than HPBCD. Actually, HPCBD is considered to be more like a bidirectional cholesterol "shuttle" rather than a "sink" in cholesterol efflux [67]. A recent paper reported that β-cyclodextrin might act as a "shuttle" at a low dose while a "sink" at a higher dose [26]. In either situation, β-cyclodextrin may only have limited cholesterol efflux or

CC-dissolving capacity without additional "sink" or "shuttle" in the system, which may explain our observation that HPBCD only exerts a minor effect in dissolving CCs or promoting cholesterol efflux. miNano seemed to have a more robust cholesterol "holding" capacity since it continued to dissolve CCs as long as 72 h while HPBCD reached saturation at 24 h.

Besides dissolving CCs directly, miNano also decreased CC-induced inflammatory responses in macrophages via inhibiting the TLR4-NF-κB pathway, corresponding to the reduced macrophage infiltration in plaques *in vivo*. Increased TLR4 expression has been identified in macrophages in both human and mouse atherosclerotic lesions [68]. Activation of the TLR4-NF-κB pathway induces inflammation and atherosclerotic plaque instability and eventually rupture. miNano treatment significantly cut down TLR4-NF-κB activation, implying that miNano may interrupt the interaction between pro-inflammatory ligands and TLR4 at the membrane. Another possible mechanism is that miNano may stabilize the cell membrane via removing excessive cholesterol, as a previous study reported that CC-induced inflammation was driven by membrane destabilization [69]. Altogether, the diminished CC burden and macrophage inflammation after miNano treatment contributed to a more stable plaque in *Ldlr*-deficient mice.

Lastly, we proved that miNano could remove CCs in human atherosclerotic plaques under a hypercholesteremia condition, in which the TC and TG levels were comparable to that of heterozygous familial hypercholesterolemia patients. Familial hypercholesterolemia is a genetic disease mainly caused by loss-of-function mutations in *Ldlr*, which leads to hypercholesteremia and resistance to statin treatment. Together with the fact that miNano prevents atherosclerosis development in *Ldlr*-deficient mice, we indicate that miNano may be a potential strategy to treat atherosclerosis in patients with familial hypercholesteremia.

Our study encompasses some limitations, which may serve as directions for future investigation. We have focused on the effect of miNano on macrophages in the setting of CCs in this study. We will further evaluate the impact of miNano on CC-induced pathology in other cells like endothelial cells and vascular smooth muscle cells, which also play important roles and are impacted by CCs in atherosclerosis development [70,71]. Second, although macrophage cholesterol efflux was studied, the effects of miNano on reverse cholesterol transport *in vivo* need to be further studied. Besides, cholesterol ester crystals may form during preparation of the frozen sections. Hence, it's difficult to distinguish the birefringence of CCs and cholesterol etser crystals. In any case, miNano decreased the "CC" signal, indicating an absolute capacity to either dissolve cholesterol ester crystals or cholesterol crystals. Last but not least, due to the technical limitation, we cannot investigate the interaction of miNano with endogenous lipoproteins *in vivo*, which will be developed in the future.

Based on its strong CC-dissolving, anti-inflammation capacity, and increased excretion of bile acids, miNano may also be promising in treating other CC-associated diseases like NASH (non-alcoholic steatohepatitis) [74–76], cholesterol embolization syndrome [77], or bile stone diseases [78], which would be worth for future research. Biomimetic nanoparticles have shown great potential in diagnosing and treating CVDs due to their biocompatibility and biodegradability [79]. Especially, macrophage membrane-coated biomimetic nanoparticles exert high targeted delivery efficiency to various inflammatory diseases, including atherosclerotic lesions [80]. The appropriate combination of phospholipid nanoparticles like miNano with selected cell-membranes may enhance the therapeutic efficacies of atherosclerosis.

In summary, we developed an HDL-based phospholipid nanoparticle, miNano, which binds to CCs directly, has CC-dissolving capability, enhances cholesterol efflux, and accumulates in atherosclerotic plaques. miNano prevents foam cell formation, suppresses inflammatory responses in macrophages, inhibits atherosclerosis, and stabilizes atherosclerotic plaques. Overall, the phospholipid nanoparticle is a promising approach to treat atherosclerosis by modulating plaque components and inhibiting inflammation.

Contributors

Conceptualization: YG, ASS, YEC; Methodology: YL, YG, MY, KH, DL, RL, BW, BY; Investigation: YL, YG, HW, DH, MY, KH, DL; Visualization: JZ, DS; Writing—original draft: YL, YG; Writing—review & editing: YL, YG, ASS, YEC. YL, YG, ASS, and YEC verified the underlying data.YL and YG share the first author position. The order was determined by order of increasing seniority. All authors have read and approved the final version of the manuscript.

Data sharing statement

The data that support the findings of this study are available from the corresponding author upon request.

Declaration of Competing Interest

The authors have declared that no conflict of interest exists.

Acknowledgments

We thank the *In Vivo* Animal Core of the Unit for Laboratory Animal Medicine at the University of Michigan (U-M) for performing the H&E and Masson's Trichrome stains. We used services from MDRC Chemistry Laboratory at U-M supported by P30DK020572 (MDRC) from the National Institute of Diabetes and Digestive and Kidney Diseases. We used ELISA services from Rogel Cancer Center's Immune Monitoring Core at U-M.

Supplementary materials

Supplementary material associated with this article can be found, in the online version, at doi:10.1016/j.ebiom.2021.103725.

References

[1] Roth GA, Johnson C, Abajobir A, Abd-Allah F, Abera SF, Abyu G, et al. Global, regional, and national burden of cardiovascular diseases for 10 causes, 1990 to 2015. J Am Coll Cardiol 2017;70(1):1–25.
[2] Khan I, Peterson ED, Cannon CP, Sedita LE, Edelberg JM, Ray KK. Time-dependent cardiovascular treatment benefit model for lipid-lowering therapies. J Am Heart Assoc 2020;9(15):e016506.
[3] Borén J, Chapman MJ, Krauss RM, Packard CJ, Bentzon JF, Binder CJ, et al. Low-density lipoproteins cause atherosclerotic cardiovascular disease: pathophysiological, genetic, and therapeutic insights: a consensus statement from the European atherosclerosis society consensus panel. Eur Heart J 2020;41(24):2313–30.
[4] Wang N, Fulcher J, Abeysuriya N, Park L, Kumar S, Di Tanna GL, et al. Intensive LDL cholesterol-lowering treatment beyond current recommendations for the prevention of major vascular events: a systematic review and meta-analysis of randomised trials including 327,037 participants. Lancet Diabetes Endocrinol 2020;8(1):36–49.
[5] Nicholls SJ, Andrews J, Kastelein JJP, Merkely B, Nissen SE, Ray KK, et al. Effect of serial infusions of CER-001, a Pre-β high-density lipoprotein mimetic, on coronary atherosclerosis in patients following acute coronary syndromes in the CER-001 atherosclerosis regression acute coronary syndrome trial: a randomized clinical trial. JAMA Cardiol 2018;3(9):815–22.
[6] Sabatine MS, Giugliano RP, Keech AC, Honarpour N, Wiviott SD, Murphy SA, et al. Evolocumab and clinical outcomes in patients with cardiovascular disease. N Engl J Med 2017;376(18):1713–22.
[7] Ridker PM, Everett BM, Thuren T, MacFadyen JG, Chang WH, Ballantyne C, et al. Antiinflammatory therapy with canakinumab for atherosclerotic disease. N Engl J Med 2017;377(12):1119–31.
[8] Nidorf SM, Fiolet ATL, Mosterd A, Eikelboom JW, Schut A, Opstal TSJ, et al. Colchicine in patients with chronic coronary disease. N Engl J Med 2020;383(19):1838–47.
[9] Nidorf SM, Eikelboom JW, Budgeon CA, Thompson PL. Low-dose colchicine for secondary prevention of cardiovascular disease. J Am Coll Cardiol 2013;61(4):404–10.

[10] Tardif JC, Kouz S, Waters DD, Bertrand OF, Diaz R, Maggioni AP, et al. Efficacy and safety of low-dose colchicine after myocardial infarction. N Engl J Med 2019;381(26):2497–505.
[11] Bouabdallaoui N, Tardif JC, Waters DD, Pinto FJ, Maggioni AP, Diaz R, et al. Time-to-treatment initiation of colchicine and cardiovascular outcomes after myocardial infarction in the colchicine cardiovascular outcomes trial (COLCOT). Eur Heart J 2020;41(42):4092–9.
[12] Janoudi A, Shamoun FE, Kalavakunta JK, Abela GS. Cholesterol crystal induced arterial inflammation and destabilization of atherosclerotic plaque. Eur Heart J 2016;37(25):1959–67.
[13] Sheedy FJ, Grebe A, Rayner KJ, Kalantari P, Ramkhelawon B, Carpenter SB, et al. CD36 coordinates NLRP3 inflammasome activation by facilitating intracellular nucleation of soluble ligands into particulate ligands in sterile inflammation. Nat Immunol 2013;14(8):812–20.
[14] Baumer Y, McCurdy S, Jin X, Weatherby TM, Dey AK, Mehta NN, et al. Ultramorphological analysis of plaque advancement and cholesterol crystal formation in Ldlr knockout mouse atherosclerosis. Atherosclerosis 2019;287:100–11.
[15] Duewell P, Kono H, Rayner KJ, Sirois CM, Vladimer G, Bauernfeind FG, et al. NLRP3 inflammasomes are required for atherogenesis and activated by cholesterol crystals. Nature 2010;464(7293):1357–61.
[16] Lehti S, Nguyen SD, Belevich I, Vihinen H, Heikkilä HM, Soliymani R, et al. Extracellular lipids accumulate in human carotid arteries as distinct three-dimensional structures and have proinflammatory properties. Am J Pathol 2018;188(2):525–38.
[17] Warnatsch A, Ioannou M, Wang Q, Papayannopoulos V. Inflammation. Neutrophil extracellular traps license macrophages for cytokine production in atherosclerosis. Science 2015;349(6245):316–20.
[18] Niyonzima N, Bakke SS, Gregersen I, Holm S, Sandanger O, Orrem HL, et al. Cholesterol crystals use complement to increase NLRP3 signaling pathways in coronary and carotid atherosclerosis. EBioMedicine 2020;60:102985.
[19] Abela GS. Cholesterol crystals piercing the arterial plaque and intima trigger local and systemic inflammation. J Clin Lipidol 2010;4(3):156–64.
[20] Abela GS, Kalavakunta JK, Janoudi A, Leffler D, Dhar G, Salehi N, et al. Frequency of cholesterol crystals in culprit coronary artery aspirate during acute myocardial infarction and their relation to inflammation and myocardial injury. Am J Cardiol 2017;120(10):1699–707.
[21] Dai J, Tian J, Hou J, Xing L, Liu S, Ma L, et al. Association between cholesterol crystals and culprit lesion vulnerability in patients with acute coronary syndrome: an optical coherence tomography study. Atherosclerosis 2016;247:111–7.
[22] Fujiyoshi K, Minami Y, Ishida K, Kato A, Katsura A, Muramatsu Y, et al. Incidence, factors, and clinical significance of cholesterol crystals in coronary plaque: an optical coherence tomography study. Atherosclerosis 2019;283:79–84.
[23] Kataoka Y, Puri R, Hammadah M, Duggal B, Uno K, Kapadia SR, et al. Cholesterol crystals associate with coronary plaque vulnerability *in vivo*. J Am Coll Cardiol 2015;65(6):630–2.
[24] Koide M, Matsuo A, Shimoo S, Takamatsu K, Kyodo A, Tsuji Y, et al. Cholesterol crystal depth in coronary atherosclerotic plaques: a novel index of plaque vulnerability using optical frequency domain imaging. PLoS One 2017;12(6):e0180303.
[25] Nishimura S, Ehara S, Hasegawa T, Matsumoto K, Yoshikawa J, Shimada K. Cholesterol crystal as a new feature of coronary vulnerable plaques: an optical coherence tomography study. J Cardiol 2017;69(1):253–9.
[26] Baumer Y, Mehta NN, Dey AK, Powell-Wiley TM, Boisvert WA. Cholesterol crystals and atherosclerosis. Eur Heart J 2020;41(24):2236–9.
[27] Patel R, Janoudi A, Vedre A, Aziz K, Tamhane U, Rubinstein J, et al. Plaque rupture and thrombosis are reduced by lowering cholesterol levels and crystallization with ezetimibe and are correlated with fluorodeoxyglucose positron emission tomography. Arterioscler Thromb Vasc Biol 2011;31(9):2007–14.
[28] Matencio A, Navarro-Orcajada S, González-Ramón A, García-Carmona F, López-Nicolás JM. Recent advances in the treatment of Niemann pick disease type C: a mini-review. Int J Pharm 2020;584:119440.
[29] Zimmer S, Grebe A, Bakke SS, Bode N, Halvorsen B, Ulas T, et al. Cyclodextrin promotes atherosclerosis regression via macrophage reprogramming. Sci Transl Med 2016;8(333):333ra50.
[30] Crumling MA, King KA, Duncan RK. Cyclodextrins and iatrogenic hearing loss: new drugs with significant risk. Front Cell Neurosci 2017;11:355.
[31] Ding D, Manohar S, Jiang H, Salvi R. Hydroxypropyl-β-cyclodextrin causes massive damage to the developing auditory and vestibular system. Hear Res 2020;396:108073.
[32] Vernon J, Brummett R, Walsh T. The ototoxic potential of propylene glycol in guinea pigs. Arch Otolaryngol 1978;104(12):726–9.
[33] Crumling MA, Liu L, Thomas PV, Benson J, Kanicki A, Kabara L, et al. Hearing loss and hair cell death in mice given the cholesterol-chelating agent hydroxypropyl-beta-cyclodextrin. PLoS One 2012;7(12):e53280.
[34] Ding D, Manohar S, Jiang H, Salvi R. Hydroxypropyl-beta-cyclodextrin causes massive damage to the developing auditory and vestibular system. Hear Res 2020;396:108073.
[35] Ben-Aicha S, Badimon L, Vilahur G. Advances in HDL: much more than lipid transporters. Int J Mol Sci 2020;21(3).
[36] Nissen SE, Tsunoda T, Tuzcu EM, Schoenhagen P, Cooper CJ, Yasin M, et al. Effect of recombinant ApoA-I milano on coronary atherosclerosis in patients with acute coronary syndromes: a randomized controlled trial. JAMA 2003;290(17):2292–300.
[37] Tardif JC, Grégoire J, L'Allier PL, Ibrahim R, Lespérance J, Heinonen TM, et al. Effects of reconstituted high-density lipoprotein infusions on coronary atherosclerosis a randomized controlled trial. JAMA 2007;297(15):1675–82.
[38] Tardif JC, Ballantyne CM, Barter P, Dasseux JL, Fayad ZA, Guertin MC, et al. Effects of the high-density lipoprotein mimetic agent CER-001 on coronary atherosclerosis in patients with acute coronary syndromes: a randomized trial†. Eur Heart J 2014;35(46):3277–86.
[39] Darabi M, Guillas-Baudouin I, Le Goff W, Chapman MJ, Kontush A. Therapeutic applications of reconstituted HDL: when structure meets function. Pharmacol Ther 2016;157:28–42.
[40] Hoang A, Drew BG, Low H, Remaley AT, Nestel P, Kingwell BA, et al. Mechanism of cholesterol efflux in humans after infusion of reconstituted high-density lipoprotein. Eur Heart J 2012;33(5):657–65.
[41] Schwendeman A, Sviridov DO, Yuan W, Guo Y, Morin EE, Yuan Y, et al. The effect of phospholipid composition of reconstituted HDL on its cholesterol efflux and anti-inflammatory properties. J Lipid Res 2015;56(9):1727–37.
[42] Jebari-Benslaiman S, Uribe KB, Benito-Vicente A, Galicia-Garcia U, Larrea-Sebal A, Alloza I, et al. Cholesterol efflux efficiency of reconstituted HDL is affected by nanoparticle lipid composition. Biomedicines 2020;8(10).
[43] Abdulla YH, Adams CWM. The action of human high density lipoprotein on cholesterol crystals Part 2. Biochemical observations. Atherosclerosis 1978;31(4):473–80.
[44] Thacker SG, Zarzour A, Chen Y, Alcicek MS, Freeman LA, Sviridov DO, et al. High-density lipoprotein reduces inflammation from cholesterol crystals by inhibiting inflammasome activation. Immunology 2016;149(3):306–19.
[45] Yuan W, Yu B, Yu M, Kuai R, Morin EE, Wang H, et al. Synthetic high-density lipoproteins delivering liver X receptor agonist prevent atherogenesis by enhancing reverse cholesterol transport. J Control Release 2021;329:361–71.
[46] Guo Y, Yuan W, Yu B, Kuai R, Hu W, Morin EE, et al. Synthetic high-density lipoprotein-mediated targeted delivery of liver X receptors agonist promotes atherosclerosis regression. EBioMedicine 2018;28:225–33.
[47] Tang J, Li D, Drake L, Yuan W, Deschaine S, Morin EE, et al. Influence of route of administration and lipidation of apolipoprotein A-I peptide on pharmacokinetics and cholesterol mobilization. J Lipid Res 2017;58(1):124–36.
[48] Guo Y, Fan Y, Zhang J, Lomberk GA, Zhou Z, Sun L, et al. Perhexiline activates KLF14 and reduces atherosclerosis by modulating ApoA-I production. J Clin Invest 2015;125(10):3819–30.
[49] Faul F, Erdfelder E, Lang AG, G*Power BA. 3: a flexible statistical power analysis program for the social, behavioral, and biomedical sciences. Behav Res Methods 2007;39(2):175–91.
[50] Fawaz MV, Kim SY, Li D, Ming R, Xia Z, Olsen K, et al. Phospholipid component defines pharmacokinetic and pharmacodynamic properties of synthetic high-density lipoproteins. J Pharmacol Exp Ther 2020;372(2):193–204.
[51] Wang H, Guo Y, Lu H, Luo Y, Hu W, Liang W, et al. Kruppel-like factor 14 deletion in myeloid cells accelerates atherosclerotic lesion development. Cardiovasc Res 2021.
[52] Harris JM, Chess RB. Effect of pegylation on pharmaceuticals. Nat Rev Drug Discov 2003;2(3):214–21.
[53] Libby P. Interleukin-1 beta as a target for atherosclerosis therapy: biological basis of CANTOS and beyond. J Am Coll Cardiol 2017;70(18):2278–89.
[54] Zidovetzki R, Levitan I. Use of cyclodextrins to manipulate plasma membrane cholesterol content: evidence, misconceptions and control strategies. Biochim Biophys Acta 2007;1768(6):1311–24.
[55] Viatour P, Merville MP, Bours V, Chariot A. Phosphorylation of NF-κB and IκB proteins: implications in cancer and inflammation. Trends Biochem Sci 2005;30(1):43–52.
[56] Pejic RN. Familial hypercholesterolemia. Ochsner J 2014;14(4):669–72.
[57] Brown A, Patel S, Ward C, Lorenz A, Ortiz M, DuRoss A, et al. PEG-lipid micelles enable cholesterol efflux in Niemann-pick type C1 disease-based lysosomal storage disorder. Sci Rep 2016;6:31750.
[58] He J, Yang Y, Zhou X, Zhang W, Liu J. Shuttle/sink model composed of β-cyclodextrin and simvastatin-loaded discoidal reconstituted high-density lipoprotein for enhanced cholesterol efflux and drug uptake in macrophage/foam cells. J Mater ChemB 2020;8(7):1496–506.
[59] Pedersbæk D, Simonsen JB. A systematic review of the biodistribution of biomimetic high-density lipoproteins in mice. J Control Release 2020;328:792–804.
[60] Váradi J, Hermenean A, Gesztelyi R, Jeney V, Balogh E, Majoros L, et al. Pharmacokinetic properties of fluorescently labelled hydroxypropyl-beta-cyclodextrin. Biomolecules 2019;9(10):509.
[61] Ishibashi S, Brown MS, Goldstein JL, Gerard RD, Hammer RE, Herz J. Hypercholesterolemia in low density lipoprotein receptor knockout mice and its reversal by adenovirus-mediated gene delivery. J Clin Invest 1993;92(2):883–93.
[62] Mahjoubin-Tehran M, Kovanen PT, Xu S, Jamialahmadi T, Sahebkar A. Cyclodextrins: potential therapeutics against atherosclerosis. Pharmacol Ther 2020;214:107620.
[63] Chen YC, Bui AV, Diesch J, Manasseh R, Hausding C, Rivera J, et al. A novel mouse model of atherosclerotic plaque instability for drug testing and mechanistic/therapeutic discoveries using gene and microRNA expression profiling. Circ Res 2013;113(3):252–65.

[64] Matoba T, Sato K, Egashira K. Mouse models of plaque rupture. Curr Opin Lipidol 2013;24(5):419–25.
[65] von der Thüsen JH, van Vlijmen BJ, Hoeben RC, Kockx MM, Havekes LM, van Berkel TJ, et al. Induction of atherosclerotic plaque rupture in apolipoprotein E-/- mice after adenovirus-mediated transfer of p53. Circulation 2002;105(17):2064–70.
[66] Singh RK, Lund FW, Haka AS, Maxfield FR. High-density lipoprotein or cyclodextrin extraction of cholesterol from aggregated LDL reduces foam cell formation. J Cell Sci 2019;132(23):jcs237271.
[67] Atger VM, de la Llera Moya M, Stoudt GW, Rodrigueza WV, Phillips MC, Rothblat GH. Cyclodextrins as catalysts for the removal of cholesterol from macrophage foam cells. J Clin Invest 1997;99(4):773–80.
[68] Xu XH, Shah PK, Faure E, Equils O, Thomas L, Fishbein MC, et al. Toll-like receptor-4 is expressed by macrophages in murine and human lipid-rich atherosclerotic plaques and upregulated by oxidized LDL. Circulation 2001;104(25):3103–8.
[69] Shu F, Chen J, Ma X, Fan Y, Yu L, Zheng W, et al. Cholesterol crystal-mediated inflammation is driven by plasma membrane destabilization. Front Immunol 2018;9.
[70] Nymo S, Niyonzima N, Espevik T, Mollnes TE. Cholesterol crystal-induced endothelial cell activation is complement-dependent and mediated by TNF. Immunobiology 2014;219(10):786–92.
[71] Corr EM, Cunningham CC, Dunne A. Cholesterol crystals activate Syk and PI3 kinase in human macrophages and dendritic cells. Atherosclerosis 2016;251:197–205.